High spin states in ^{181}Ir and backbending phenomena in the Os-Pt region

R. Kaczarowski*
Physics Department, University of Notre Dame, Notre Dame, Indiana 46556
and Soltan Institute for Nuclear Studies, 05-400 Swierk, Poland

U. Garg, E. G. Funk, and J. W. Mihelich
Physics Department, University of Notre Dame, Notre Dame, Indiana 46556
(Received 12 July 1991)

The ^{169}Tm(^{16}O,4n)^{181}Ir reaction has been employed to investigate the high spin states of ^{181}Ir using in-beam γ spectroscopy. A well-developed system of levels built on the $h_{9/2}$ subshell was identified up to a maximum spin of $(\frac{41}{2}^-)$. Two rotational bands built on the isomeric states with $\tau_{1/2}=0.33$ μs ($E_x=289.2$ keV) and 0.13 μs ($E_x=366.2$ keV), respectively, were observed. The deduced g_K values of 1.19 ± 0.11 and 1.50 ± 0.12 indicate Nilsson assignments of $\frac{9}{2}^-[514]$ and $\frac{5}{2}^+[402]$, respectively, for the bandheads of these bands. A high spin ($I\geq\frac{19}{2}$) isomer with $\tau_{1/2}=22$ ns was found at an excitation energy above 1.96 MeV. The experimental results are discussed in terms of rotational models including Coriolis coupling and providing for a stable triaxial shape of the ^{181}Ir nucleus.

PACS number(s): 23.20.−g, 27.70.+q, 21.10.Re

I. INTRODUCTION

The iridium isotopes lie in the region of transition between deformed and spherical nuclei. Therefore, it is not expected that any of the extreme models, the Nilsson model or the spherical shell model, will provide a good description of the nuclear states. However, it is possible to find Nilsson model assignments which account for the main properties of these nuclei. Some unusual properties, such as triaxiality or shape coexistence, may arise due to softness of the nuclear potential and its consequent sensitivity to particle configuration and to particle alignment.

In-beam study of ^{181}Ir, undertaken at the University of Notre Dame Nuclear Structure Laboratory, extends the investigation of the odd-A ($A=183-191$) Ir isotopes initiated by the INR Swierk (Poland)–ISN Grenoble (France) Collaboration [1–4]. Preliminary data on backbending in the $\frac{1}{2}^-[541]$ band in ^{181}Ir has been published previously [5]; also, data on the lifetimes of high spin states in ^{181}Ir and ^{180}Os obtained in this collaboration have been published in a separate paper [6].

Only preliminary data [7] on the radioactive decay ^{181}Pt$\rightarrow$^{181}Ir were available prior to this work. Very recently, some data on ^{181}Ir were published by Kreiner *et al.* [8]. In addition to several levels from the yrast and yrare bands already known from our previous work [5,6], they have identified eight levels built on a 190 ± 60 ns isomer. The present paper summarizes the level properties of ^{181}Ir studied in the (^{16}O, 4n) reaction. A level system built on the $h_{9/2}$ subshell is identified. The existence of two strongly coupled rotational bands built on low-lying isomeric states, tentatively assigned to $\frac{9}{2}^-[514]$ and $\frac{5}{2}^+[402]$ Nilsson states, has also been established. Another level system, built on a high spin ($I\geq\frac{19}{2}$) isomeric state with $E\geq1.96$ MeV and decaying to the proposed $\frac{9}{2}^-[514]$ rotational band, was also identified.

Results of attempts to deduce the shape of the nucleus from the analysis of the $h_{9/2}$ level system in terms of the axially symmetric rotational model including the Coriolis coupling and pairing interaction, and the extended asymmetric rotor model are presented. The backbending behavior of the rotational bands in ^{181}Ir is also discussed and compared with the neighboring nuclei.

II. EXPERIMENTAL PROCEDURES AND DATA ANALYSIS

A. Targets and reaction

The reaction ^{169}Tm(^{16}O,xn)$^{185-x}$Ir was employed using projectile energies ranging from 76 to 84 MeV provided by the Notre Dame three-stage FN accelerator. The maximum beam energy was limited by the highest stable voltage available at the terminal of the FN tandem. The lowest energy was close to the Coulomb barrier for the fusion reaction. Self-supporting, thin (~3 mg/cm^2), metallic Tm targets were used.

B. Excitation functions

Measurements of the excitation function were performed at beam energies of 78, 79.5, 81, 82.5, and 84 MeV. A run at 76-MeV beam energy allowed identification of γ rays following the Coulomb excitation of the target. After each run the γ-ray spectra from induced target radioactivity were also recorded. A Ge(Li) detector with an active volume of ~100 cm^3 was positioned at 55° with respect to the beam axis. The integrated beam current values for each run were used for nor-

*Permanent address: Soltan Institute for Nuclear Studies, 05-400 Swierk, Poland.

malization purposes. The assignment of γ-ray transitions to $4n$ and $3n$ channels leading to ^{181}Ir and ^{182}Ir, respectively, was made on the basis of correlations of excitation functions with the yields of daughter nuclei in $A=181$ and 180 chains, corrected for accumulation of radioactivity of long-lived isotopes. The yield of the $2n$ reaction channel was found to be negligible. Examples of excitation functions for several transitions assigned to $4n$ and $3n$ channels are shown in Fig. 1. The relative yields of different γ transitions from the $4n$ channel were also used as an indication of the location of a transition in the level scheme of the daughter nucleus, as the excitation functions are sensitive to the spin of the emitting level. It can be seen from Fig. 1 that the maximum cross section for the $4n$ reaction channel was not reached due to the limited available beam energy; the maximum available beam energy, 84 MeV, was used for angular distributions and coincidence measurements. The energies and relative intensities (at 84-MeV beam energy) of transitions assigned to ^{181}Ir are given in Table I. The uncertainty in the transition energies is estimated to be of order of 0.2 keV, although the relative energies of strong transitions are determined with an accuracy better than 0.1 keV.

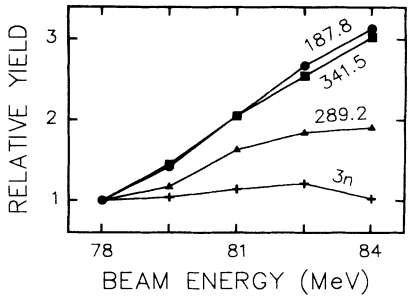

FIG. 1. Relative yields of three selected γ transitions in ^{181}Ir and the sum of several strongest γ transitions assigned to the $3n$ reaction channel.

C. Angular distributions

γ spectra were recorded at 0°, 24°, 35°, 45°, 55°, 66°, and 90° relative to the incident beam direction in order to determine the angular distributions at the beam energy of 84 MeV. The γ-ray intensities were corrected for absorption in the target and the lead stopper used in these measurements. The strongest γ rays recorded by an addition-

TABLE I. Only transitions assigned to ^{181}Ir are listed. *Y*, transition assigned to the $h_{9/2}$ system or observed in coincidence with transitions assigned to this system; *A*, transition observed in coincidence spectrum gated by the delayed 341.5-keV transition; *B*, transition observed in coincidence spectrum gated by the delayed 289.2 keV transition; and *C*, delayed transition observed in coincidence with rotational transitions above the low-lying isomers.

E_γ (keV)	Identification	I_γ	I_{tot}	$I_\gamma^{84\,MeV}/I_\gamma^{78\,MeV}$	A_2/A_0	A_4/A_0
103.7	$B\ \frac{7}{2}^+\rightarrow\frac{5}{2}^+$	3.4(7)	23.1			
117.2	$A\ \frac{11}{2}^-\rightarrow\frac{9}{2}^-$	9.7(22)	12,34,49			
128.7	$B\ \frac{9}{2}^+\rightarrow\frac{7}{2}^+$	6.2(8)	25.6			
139.8	A	1.8(5)	2,4,6		0.0(4)	−0.3(6)
151.6	$B\ \frac{11}{2}^+\rightarrow\frac{9}{2}^+$	6.4(8)	19.0	1.6(3)	−0.15(6)	0.09(9)
157.4	A 2118.3→1961.0	5.1(5)	6,9,14		0.11(14)	0.00(16)
171.0	$A\ \frac{13}{2}^-\rightarrow\frac{11}{2}^-$	27.5(20)	66.1	4.4(3)	0.07(3)	0.00(4)
171.5	$B\ \frac{13}{2}^+\rightarrow\frac{11}{2}^+$	8.5(8)	20.3			
183.5	$A\ \frac{15}{2}^-\rightarrow\frac{13}{2}^-$	22.7(17)	48.8	2.8(3)	0.10(2)	0.05(2)
187.8	$Y\ \frac{13}{2}^-\rightarrow\frac{9}{2}^-$	100.0(20)	143.5	3.1(1)	0.32(3)	−0.08(4)
190.5	A 2308.9→2118.3	4.6(5)	5,6,9	1.5(3)	0.29(10)	−0.02(12)
190.6	$B\ \frac{15}{2}^+\rightarrow\frac{13}{2}^+$	7.4(8)	15.0			
203.1	$A\ \frac{17}{2}^-\rightarrow\frac{13}{2}^-$	18.3(15)	34.1	3.4(3)	0.10(3)	−0.06(4)
204.2	$B\ \frac{17}{2}^+\rightarrow\frac{15}{2}^+$	5.8(8)	10.7			
215.4	A 2524.4→2308.9	5.3(5)	6,7,9	3.5(4)	0.27(5)	−0.15(7)
215.6	$A\ \frac{19}{2}^-\rightarrow\frac{17}{2}^-$	14.5(15)	25.1			
219.4	$B\ \frac{19}{2}^+\rightarrow\frac{17}{2}^+$	4.2(6)	7.1			
227.9	$B\ \frac{21}{2}^+\rightarrow\frac{19}{2}^+$	2.6(5)	4.2			
230.0	$A\ \frac{21}{2}^-\rightarrow\frac{19}{2}^-$	7.4(7)	11.9	2.4(3)		
232.4	$B\ \frac{9}{2}^+\rightarrow\frac{5}{2}^+$	1.5(4)	1.8			
236.1	A 2760.5→2524.4	2.2(4)	2.3+3.5		−0.2(3)	0.4(3)
240.1	$A\ \frac{23}{2}^-\rightarrow\frac{21}{2}^-$	5.7(6)	8.9		0.15(15)	0.15(16)
241.1	$B\ \frac{23}{2}^+\rightarrow\frac{21}{2}^+$	1.9(4)	2.9			
249.7	$B\ \frac{25}{2}^+\rightarrow\frac{23}{2}^+$	1.2(3)	1.8			
251.7	$A\ \frac{25}{2}^-\rightarrow\frac{23}{2}^-$	3.0(5)	4.4		0.12(10)	0.16(12)

TABLE I. (*Continued*).

E_γ (keV)	Identification	I_γ	I_{tot}	$I_\gamma^{84\,MeV}/I_\gamma^{78\,MeV}$	A_2/A_0	A_4/A_0
254.0	*A* 3014.5→2760.5	2.3(6)	2.4+4.5		0.35(13)	0.02(15)
261.1	*A* $\frac{27}{2}^- \rightarrow \frac{25}{2}^-$	2.8(5)	4.0		−0.08(14)	0.07(18)
263.6	*B* $\frac{27}{2}^+ \rightarrow \frac{25}{2}^+$	1.3(3)	1.8		−0.34(17)	0.18(20)
267	*Y* $\frac{15}{2}^- \rightarrow \frac{17}{2}^-$	2(1)				
272	*B* $(\frac{29}{2}) \rightarrow \frac{27}{2}^+$	0.7(2)	1.0			
272.8	*A* $\frac{29}{2}^- \rightarrow \frac{27}{2}^-$	2.0(4)	2.8			
280.3	*B* $\frac{11}{2}^+ \rightarrow \frac{7}{2}^+$	3.4(4)	3.8		0.8(7)	−0.4(7)
283.3	*A* $(\frac{31}{2}) \rightarrow \frac{29}{2}^-$	3.0(4)	4.0			
285.4	*C* $\frac{7}{2}^- \rightarrow \frac{9}{2}^-$	3.3(4)	4.4			
286.3	*Y* $(\frac{11}{2}^-) \rightarrow \frac{13}{2}^-$	2.5(10)				
288.4	*A* $\frac{13}{2}^- \rightarrow \frac{9}{2}^-$	3.2(5)	3.3+4.2			
289.2	*C* $\frac{5}{2}^+ \rightarrow \frac{5}{2}^-$	40.2(11)	41.3	1.9(2)	0.02(3)	0.03(4)
295.2	*Y* $(\frac{21}{2}) \rightarrow (\frac{17}{2})$	23.0(23)	25.3	1.8(2)	0.13(3)	0.05(4)
296.1	*A* $(\frac{33}{2}) \rightarrow (\frac{31}{2})$	1.1(3)	1.4			
310.1	*C* $\frac{7}{2}^- \rightarrow \frac{5}{2}^-$	3.8(5)	4.8		−0.2(5)	0.0(3)
318.1	*A*	7.2(7)	7.4+9.0	2.3(2)	−0.08(5)	0.04(6)
323.1	*B* $\frac{13}{2}^+ \rightarrow \frac{9}{2}^+$	5.1(7)	5.5	0.9(2)	−0.07(11)	−0.10(15)
332.0	*A*	4.0(4)	4.1+4.9	2.5(7)	−0.14(8)	−0.02(10)
335.6	*Y* $\frac{17}{2}^- \rightarrow \frac{13}{2}^-$	99.9(15)	106.8	3.2(1)	0.26(2)	−0.08(3)
341.5	*C* $\frac{9}{2}^- \rightarrow \frac{9}{2}^-$	70.9(12)	72,76,86	3.0(1)	0.02(3)	−0.02(3)
354.5	*A* $\frac{15}{2}^- \rightarrow \frac{11}{2}^-$	8.7(8)	9.2		0.51(12)	−0.40(15)
362.0	*B* $\frac{15}{2}^+ \rightarrow \frac{11}{2}^+$	6.4(8)	6.8		−0.06(5)	−0.07(5)
365.9	*Y* $(\frac{17}{2}) \rightarrow (\frac{15}{2})$	2.3(6)	≤2.7			
366.2	*C* $\frac{9}{2}^- \rightarrow \frac{5}{2}^-$	2.0(2)	2.1			
376.8	*A*	4.6(6)	4.7,4.8,5.3		0.1(3)	0.1(4)
380.2	*A*	1.5(5)	1.5,1.6,1.7		−0.5(3)	0.4(3)
385.1	*Y* $(\frac{25}{2}) \rightarrow (\frac{21}{2})$	19.5(20)	20.2	7.2(18)	0.26(6)	0.05(7)
386.6	*A* $\frac{17}{2}^- \rightarrow \frac{13}{2}^-$	14.2(11)	14.9	3.1(8)	0.08(8)	0.09(11)
394.6	*B* $\frac{17}{2}^+ \rightarrow \frac{13}{2}^+$	7.8(9)	8.1		0.36(8)	−0.07(9)
406.1	*A* 2524.4→2118.3	1.6(4)	1.6+1.8			
418.7	*A* $\frac{19}{2}^- \rightarrow \frac{15}{2}^-$	10.9(8)	11.3	5.5(11)	0.19(7)	−0.19(8)
421.6	*A*	3.6(5)	3.6+4			
423.7	*B* $\frac{19}{2}^+ \rightarrow \frac{15}{2}^+$	6.2(7)	6.4	5.1(18)	0.36(11)	−0.10(13)
431	*Y* $\frac{19}{2}^- \rightarrow \frac{15}{2}^-$	4.3(9)			−0.17(17)	−0.08(17)
431.7	*Y* $(\frac{21}{2}) \rightarrow \frac{19}{2}^-$					
432.8	*Y* $(\frac{29}{2}) \rightarrow (\frac{25}{2})$	7.6(15)			0.23(15)	−0.10(15)
445.6	*A* $\frac{21}{2}^- \rightarrow \frac{17}{2}^-$	8.6(10)	8.9	3.2(8)	0.47(10)	0.18(12)
447.2	*B* $\frac{21}{2}^+ \rightarrow \frac{17}{2}^+$	5.3(6)	5.5		0.4(5)	0.7(7)
451.5	*A* 2760.5→2308.9	2.6(4)	2.6+2.9		0.19(13)	−0.5(3)
455.8	*Y* $\frac{21}{2}^- \rightarrow \frac{17}{2}^-$	59.3(15)	61.1	4.2(4)	0.37(3)	−0.14(4)
466.9	*Y* $(\frac{15}{2}) \rightarrow \frac{17}{2}^-$	7.2(15)	≤7.8		0.11(12)	0.02(15)
469.0	*B* $\frac{23}{2}^+ \rightarrow \frac{19}{2}^+$	4.1(7)	4.2		0.19(9)	0.0(1)
470.1	*A* $\frac{23}{2}^- \rightarrow \frac{19}{2}^-$	7.0(6)	7.2			
474.5	*Y* $(\frac{11}{2}^-) \rightarrow \frac{9}{2}^-$	4(2)				
490.1	*A* 3014.5→2524.4	3.0(7)	3.0+3.2			
490.8	*B* $\frac{25}{2}^+ \rightarrow \frac{21}{2}^+$	3.9(6)	4.0		0.32(7)	−0.06(8)
491.7	*A* $\frac{25}{2}^- \rightarrow \frac{21}{2}^-$	5.3(5)	5.4			
512.6	*B* $\frac{27}{2}^+ \rightarrow \frac{23}{2}^+$	4.1(10)	4.2			
512.8	*A* $\frac{27}{2}^- \rightarrow \frac{23}{2}^-$	7.3(20)	7.4			
517.9	*Y* $\frac{23}{2}^- \rightarrow \frac{19}{2}^-$	7.1(15)	7.2		?0.7(14)	−0.4(14)
533.8	*A* $\frac{29}{2}^- \rightarrow \frac{25}{2}^-$	4.6(6)	4.7		0.48(9)	0.0(1)
535.6	*B* $(\frac{29}{2}) \rightarrow \frac{27}{2}^+$	2.4(6)	2.4			
545.7	*Y* $\frac{25}{2}^- \rightarrow \frac{21}{2}^-$	38.2(15)	38.9	3.7(4)	0.30(5)	−0.08(6)

TABLE I. (*Continued*).

E_γ (keV)	Identification	I_γ	I_{tot}	$I_\gamma^{84\,MeV}/I_\gamma^{78\,MeV}$	A_2/A_0	A_4/A_0
556.1	$A\ (\frac{31}{2})\rightarrow\frac{27}{2}^-$	3.6(6)	3.7			
565.9	$Y\ (\frac{17}{2})\rightarrow\frac{15}{2}^-$	9.0(10)	9.1	3.4(6)	−0.28(8)	0.47(10)
570.0	$Y\ \frac{37}{2}^-\rightarrow\frac{33}{2}^-$	6.3(12)	6.4		?0.13(8)	0.18(10)
579.8	$A\ (\frac{33}{2})\rightarrow\frac{29}{2}^-$	3.0(6)	3.0			
597.8	$Y\ \frac{27}{2}^-\rightarrow\frac{23}{2}^-$	10.6(20)	10.8		−0.02(12)	−0.06(13)
600	$Y\ (\frac{41}{2}^-)\rightarrow\frac{37}{2}^-$	6.0(15)	6.1			
602.3	$Y\ \frac{15}{2}^-\rightarrow\frac{13}{2}^-$	14.6(12)	15.3	3.2(5)	−0.41(8)	0.03(9)
603.6	A	4.0(10)	4.0			
604.8	$Y\ \frac{29}{2}^-\rightarrow\frac{25}{2}^-$	25.7(15)	26.1	5.3(9)	0.33(4)	−0.14(5)
621.2	$Y\ \frac{33}{2}^-\rightarrow\frac{29}{2}^-$	10.3(15)	10.4	7.1(15)	0.14(10)	0.02(10)
625.4	$A\ (\frac{21}{2}^-)\rightarrow\frac{19}{2}^-$	9.2(8)	9.2+9.6	2.3(5)	−0.19(8)	0.16(9)
672.0	$Y\ (\frac{21}{2})\rightarrow\frac{21}{2}^-$	8.0(15)	8.0		0.21(15)	−0.1(2)
696.1	$Y\ \frac{19}{2}^-\rightarrow\frac{17}{2}^-$	11.0(20)	11.4	3.3(6)	−0.51(9)	0.22(11)
704.4	A	2.0(5)	2.0			
758.3	$Y\ \frac{23}{2}^-\rightarrow\frac{21}{2}^-$	9.8(20)	10.0		−0.59(14)	0.16(15)
802.4	$Y\ (\frac{15}{2})\rightarrow\frac{13}{2}^-$	5.9(12)	6.0	4.1(10)	?0.13(4)	0.10(5)
810.2	$Y\ \frac{27}{2}^-\rightarrow\frac{25}{2}^-$	7.8(14)	8.0	2.8(7)	0.22(12)	−0.25(14)
832.5	$Y\ (\frac{17}{2})\rightarrow\frac{17}{2}^-$	11.0(15)	11.0		0.19(9)	−0.08(10)
914.9	A 1955.9$\rightarrow\frac{17}{2}^-$	3.5(6)	3.5			
919.9	A 1961.0$\rightarrow\frac{17}{2}^-$	5.7(7)	5.7		−0.03(13)	0.09(14)
1117.7	A 1955.9$\rightarrow\frac{15}{2}^-$	1.5(4)	1.5			
1123.0	A 1961.0$\rightarrow\frac{15}{2}^-$	2.9(6)	2.9			

al Ge(Li) detector placed at a fixed angle of 90°, as well as the isotropic K-X radiation, were used for normalization. The angular distribution was fitted with a Legendre polynomial and the distribution coefficients A_2/A_0 and A_4/A_0 were extracted from these fits. The ratios A_K/A_0 may be expressed as a product of two factors A_K^{max}/A_0 and α_K, where A_K^{max}/A_0 corresponds to the completely aligned case and α_K express the degree of alignment. If $\alpha_K(I)$ for a state can be determined from a pure transition, conclusions about multipolarities and spin sequences can be drawn, as discussed by der Mateosian and Sunyar [9]. The angular distribution coefficients of the strongest stretched $E2$ transitions in the decoupled yrast band were used for this purpose. The angular distribution coefficients extracted for the γ rays belonging to ^{181}Ir are also given in Table I.

D. Coincidence and lifetime measurements

γ-γ-t coincidence measurements were performed at beam energies of 84 and 78 MeV with two Ge(Li) detectors (104 and 90 cm^3) placed symmetrically at about $\pm 120°$ relative to the beam. The size of the coincidence matrix was $4096\times4096\times512$, covering 0.7 μs in the time dimension. Great care was taken to reduce the random coincidence background and the possibility of backscattering of the γ rays from one detector to the other. The resulting time resolution (FWHM of the prompt coincidence peak in the time cross sections) varies from 9 to 16 ns for γ-ray energies from 1.3 down to 0.2 MeV, respectively. The coincidence events were stored on magnetic tapes and sorted off line. A total of approximately 39×10^6 coincidence events were gathered at 84 MeV. An additional 12×10^6 events recorded at the beam energy of 78 MeV were very helpful in assignments of particular γ cascades to $4n$ and $3n$ reaction channels.

The timing information from the γ-γ-t coincidence matrix was used to extract the lifetimes of the individual γ transitions in the ns region. The slope of the prompt-coincidence peak in the time-distribution spectra determined the lower limit of about 10 ns for the measured half-lives; the upper limit was set to about 1 μs by the range of the TAC. Three isomers with half-lives in the ns range were found. The measured half-lives for the 341.5- and 289.2-keV isomeric transitions were 126±6 ns and $0.33^{+0.10}_{-0.06}$ μs, respectively; the former value is consistent with the half-life of 190±60 ns reported by Kreiner *et al.* [8]. An isomer with high excitation energy and a half-life of 22±4 ns, calculated as a mean value of measured half-lives of the 625.4-, 171.0-, 183.5-, and 203.1-keV transitions, was also observed.

Figure 2 shows the examples of the background corrected prompt- and delayed-coincidence spectra. The yrast band can be traced up to a spin of $(\frac{41}{2}^-)$, while two other bands, built on low-lying isomeric states, have been observed up to spin of $(\frac{33}{2})$ and $(\frac{29}{2})$, respectively.

III. EXPERIMENTAL RESULTS

A. The level scheme of ^{181}Ir

The level scheme of ^{181}Ir, deduced from the present experiment, is shown in Fig. 3. The assignments of Nilsson

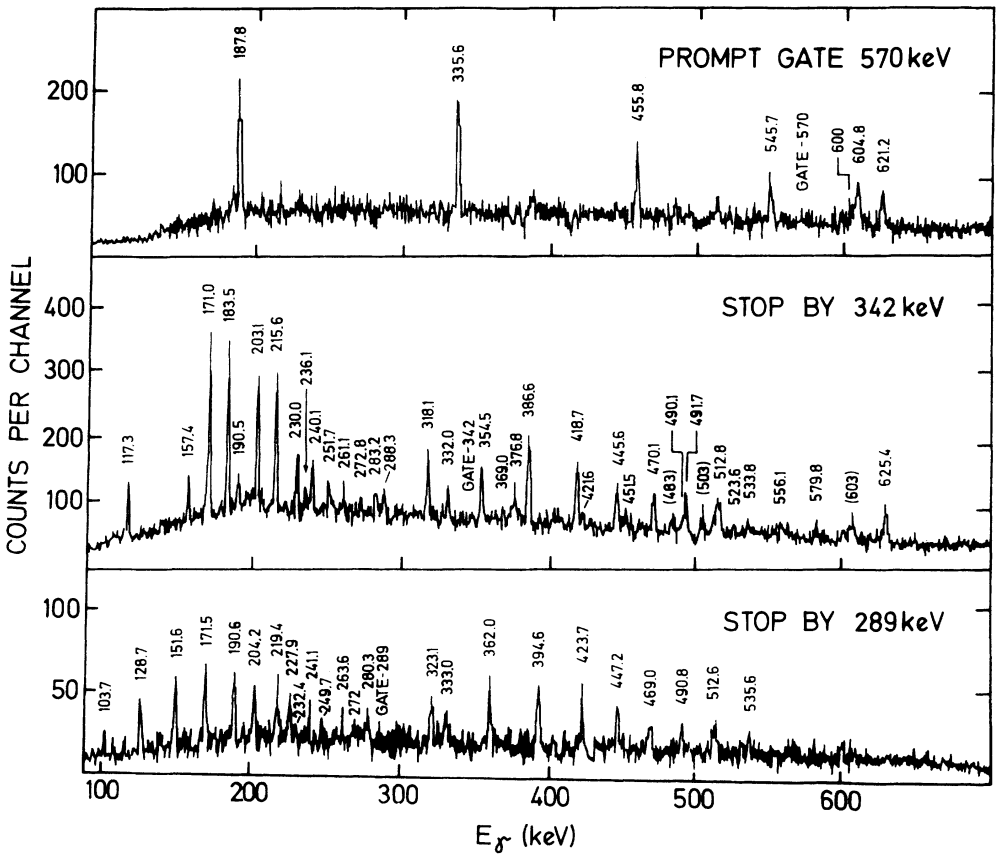

FIG. 2. Background-corrected prompt and delayed γ coincidence spectra for three bands in ^{181}Ir. Gates have been set on individual γ lines as indicated.

orbitals to the bands as well as the spin assignments will be discussed for each band in the next subsections. Uncertain spin and parity assignments are indicated in Fig. 3 by brackets and the inferred, but not observed, transitions, as well as transitions for which only weak evidence is known, are shown in the level scheme by dashed lines. Table I contains spectroscopic information on the transitions assigned to the $4n$ reaction channel leading to ^{181}Ir.

B. The ground-state rotational band (g.s.b.) and related levels

The strongest γ-ray cascade observed in our study is comprised of stretched $E2$ transitions, as deduced from angular distribution data. In accordance with the relative yields and excitation functions, these transitions were used to construct a decoupled ground-state rotational band. The only proton orbital close to the Fermi level in this nuclear region which can be the bandhead of a decoupled rotational band is the $\frac{1}{2}^-[541]$ Nilsson orbital, as has been observed in heavier odd-A ($A=183-189$) Ir isotopes [1–3]. Due to the relatively large decoupling factor, $a \approx 4$, of this orbital [10], the $\frac{5}{2}^-$ rotational state is expected to be the lowest member of the rotational band. A direct spin measurement [11] of $\frac{5}{2}$ for the ground state of ^{185}Ir has been interpreted in this way [12]. In addition, the observed level spacings fit smoothly into systematics of the $\frac{1}{2}^-[541]$ bands [13]. The combination of the measured g.s. spin, the stretched $E2$ transitions, and the systematics has formed the basis for the spin assignments in the g.s.b. up to the $I=(\frac{41}{2}^-)$ state. The angular distribution data for the highest (600-keV) transition cannot confirm its stretched $E2$ character, however, because of its low intensity, and an $E2$ character has been assumed based on the information available from a separate experiment [5]. According to the systematics, the lowest $\frac{9}{2}^- \rightarrow \frac{5}{2}^-$ transition is expected to have an energy of about 25 keV and, consequently, could not be observed directly in the present study. However, four delayed transitions observed in the decay of the $\tau_{1/2}=126$ ns isomer, viz., 285.4, 310.1, 341.5, and 366.2 keV, may be grouped into two pairs having, within experimental errors of the order of 0.1 keV, exactly the same energy difference of 24.7 keV. These transitions are not in coincidence with each other. The time distribution of the 341.5-keV transition (which is also the strongest) shows no prompt component and, hence, has to directly deexcite the isomeric level. Therefore, it seems reasonable to assume that these transitions deexcite two levels with energies 310.1 and 366.2 keV to the $\frac{9}{2}^-$ and $\frac{5}{2}^-$ members of the g.s.b., thus establishing their energy difference as 24.7 keV, in very good agreement with the expected value and with preliminary data of Schück *et al.* [7].

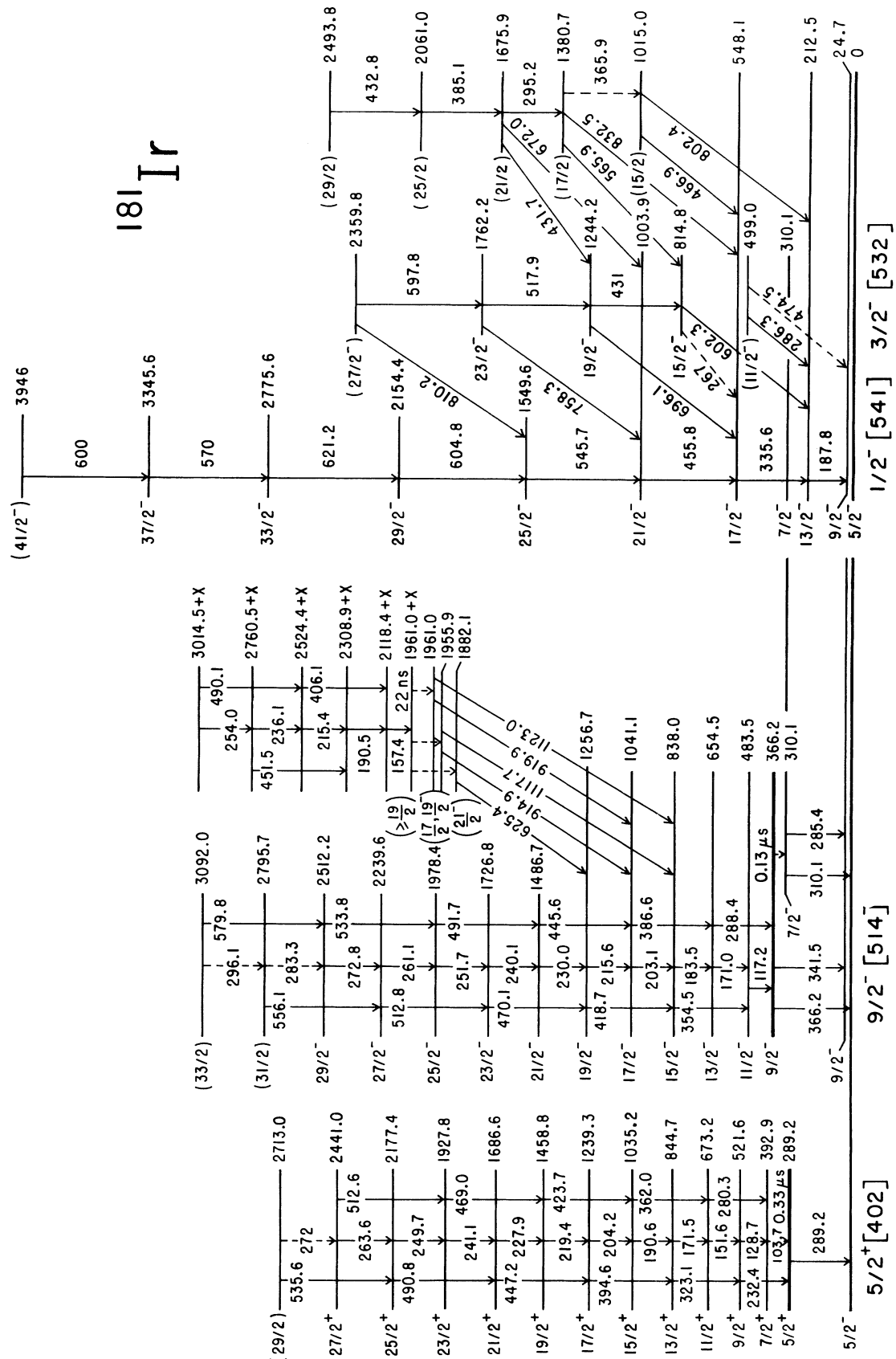

FIG. 3. Level scheme of ^{181}Ir deduced from the present work.

The $\frac{7}{2}^-$ state observed in ^{183}Ir at 329.0 keV decays to the $\frac{5}{2}^-$ and $\frac{9}{2}^-$ members of the g.s.b. with branching ratio $[I_\gamma(\frac{7}{2}^- \rightarrow \frac{5}{2}^-)/I_\gamma(\frac{7}{2}^- \rightarrow \frac{9}{2}^-)]$ of 0.78. A comparable branching ratio of 0.87 ± 0.15 is observed for analogous decay of the proposed 310.1-keV state. Therefore, we propose an assignment of spin and parity of $\frac{7}{2}^-$ for the 310.1-keV level, in agreement with results of analysis of the decay pattern of the 366.3-keV state (see next subsection). The hindrance factors relative to the Weisskopf estimates for the $E2$ transition from the 366.2-keV isomeric state to the $\frac{5}{2}^-$, $\frac{7}{2}^-$, and $\frac{9}{2}^-$ states are 3.9×10^3, 5.4, and 76, respectively, indicating not only increasing admixtures of higher-K components of the $h_{9/2}$ proton orbital into wave functions of these states but also a different nature of the $\frac{7}{2}^-$ level. Indeed, the Coriolis coupling calculations (see Sec. IV B) indicate that the wave function of the pure Nilsson state of $\frac{1}{2}^-[541]$ is the main admixture into the wave functions of the $\frac{5}{2}^-$ and $\frac{9}{2}^-$ rotational states, while the $\frac{3}{2}^-[532]$ wave function constitutes the main component of the wave functions of $\frac{7}{2}^-$ rotational level and other yrare band states.

A weak 286.3-keV transition seen in coincidence with the 187.8-keV yrast transition together with another weak 474.5-keV transition may place a possible $\frac{11}{2}^-$ yrare level at 499.0 keV; very weak feeding to this level does not allow a direct confirmation of this proposed assignment, however. The higher-placed yrare band levels decay to the g.s.b. by strong, mixed, $M1/E2$ ($\Delta I=\pm1$) transitions, as deduced from angular distribution data. The absence of an observable, energetically favored, transition to the $\frac{9}{2}^-$ yrast state and the increasing-spin rule indicate a $\frac{15}{2}^-$ spin and parity assignment for the 814.8-keV state. The spin and parity assignments for two higher members of this band were made in an analogous way. The angular distribution data for the 810.2-keV transition are inconsistent with its $\Delta I=-1$ character inferred from its placement in the level scheme and, therefore, the proposed $\frac{27}{2}^-$ assignment for the 2359.8-keV level is somewhat uncertain.

The 1015.0-keV level decays only to the $\frac{13}{2}^-$ and $\frac{17}{2}^-$ members of the yrast band. Positive values of A_2 and A_4 coefficients for the 802.4-keV transition suggest its $\Delta I=\pm1$ character and, therefore, a spin value of $\frac{15}{2}$ is proposed tentatively for the 1015.0-keV state.

Another set of four levels seems to form a rotational band with the lowest observed state at 1380.7 keV. The measured values of A_2 and A_4 angular distribution coefficients for three cascade transitions are consistent with an assumption of their stretched $E2$ character, although the lower value of A_2 for the 295.2-keV transition cannot exclude $\Delta I=\pm1$. Two lowest levels of the proposed band decay to yrast and yrare states. In the following discussion of spin-parity assignments for these levels, we will assume that the depopulating transition may have only $E1$, $M1$, or $E2$ character. This assumption is supported by the measured value of the partial mean lifetime of $\tau=38\pm13$ ps for the interband 672.0-keV transition from the rotational level of 1675.9 keV which clearly excludes $M2$, $E3$, and higher multipolarities for this transition. Resulting hindrance factors relative to the Weisskopf estimates, assuming $E1$, $E2$, and $M1$ multipolarity of this transition, would be 3.7×10^4, 0.4, and 3.6×10^2, respectively; all these values are quite typical of this nuclear region.

The 1380.7-keV level decays to the $\frac{15}{2}^-$ and $\frac{17}{2}^-$ levels of the yrare and yrast bands, respectively, leading to possible spin assignments from $\frac{13}{2}$ to $\frac{19}{2}$ with negative parity, or $\frac{15}{2}$ and $\frac{17}{2}$ with positive parity under the aforementioned assumption of the $E1$, $M1$, or $E2$ character of the depopulating transitions. From these possibilities, the value of $A_2(566\text{ keV})=-0.28\pm0.08$ excludes, within about 6σ, the $\frac{15}{2}^+$ and $\frac{19}{2}^-$ assignments [the former also excluded, within 3σ, by the value of A_2 (832 keV)$=0.19\pm0.09$], thus limiting the choice of the assignments to $\frac{13}{2}^-$, $\frac{15}{2}^-$, and $\frac{17}{2}$ with either parity. The first two values are disfavored by the increasing spin rule; the lack of deexciting transitions to the $\frac{11}{2}^-$ and $\frac{13}{2}^-$ yrare and yrast states, respectively, while not a strong argument, nevertheless favors the $I=\frac{17}{2}^+$ assignment for the 1380.7-keV level. The 565.9-keV transition would, then, be $E1$ with A_4 (566 keV)$=0$ in contradiction with the measured value of A_4 (566)$=0.47\pm0.10$. However, in this particular case, the χ^2 value of the fit of angular distribution coefficients is large, indicating a possible systematic error or contamination of this transition. Similar considerations for the next level at 1675.9 keV, where the values of $A_2(672)>0$ and $A_4(672)<0$ slightly favor $\Delta I=0$ for the 672-keV transition, indicate a spin of $\frac{21}{2}$ with either parity; an absence of transition to the $\frac{17}{2}^-$ yrast state would favor positive parity. However, it would be difficult to explain no noticeable interaction (no interband transitions were observed) between the proposed $\frac{21}{2}^+$ level at 1675.9 keV and the close-lying ($\Delta E\approx11$ keV) $\frac{21}{2}^+$ member of the $\frac{5}{2}^+[402]$ rotational band (see Sec. III E). Since the rejection of the negative-parity assignment is based on rather weak arguments—the absence of some expected transitions to the yrare and yrast bands—only a tentative spin assignment with no definite parity can be made for these levels on the basis of available experimental data.

C. The $\frac{9}{2}^-[514]$ rotational band and related levels

More than 30 transitions, most of them forming a strongly coupled rotational band, are seen in the delayed coincidence gate set on the 341.5-keV transition depopulating the isomeric ($\tau_{1/2}=126\pm6$ ns) level at 366.2 keV (see Fig. 2 and discussion in the previous subsection). The strongest of them are seen also in the delayed coincidence gates set on the 285.4 and 310.2-keV transitions, indicating that the 310.1-keV state is fed mainly from the 366.2-keV isomer. An intensity balance of the transitions feeding and depopulating the 366.2-keV state leads to a value of $\alpha_{\text{tot}}=-0.01\pm0.04$ for the total internal conversion coefficient (ICC) of the 341.5-keV transition, limiting its multipolarity, within 2 standard deviations, to $E1$ (calculated [14] $\alpha_{\text{tot}}^{\text{th}}=0.019$) or $E2$ ($\alpha_{\text{tot}}^{\text{th}}=0.066$) with small $M1$ ($\alpha_{\text{tot}}^{\text{th}}=0.208$) admixture. The strongest unplaced transition (318.1 keV) seen in the delayed 341.5-keV coin-

cidence gate was assumed to feed the isomeric state directly (or via unseen cascade transitions). Other unplaced transitions are either in coincidence with transitions taken into account in intensity balance or are weak enough to be covered by experimental errors. If no enhancement relative to Weisskopf estimates is assumed, the measured half-life of this isomer allows for only $E1$, $M1$-$E2$, or $M2$ multipolarity for the depopulating transitions with the last possibility clearly excluded for the 341.5-keV transition by its ICC value. Therefore, the only possible spin and parity assignments for the 366.2-keV level, consistent with its decay to the $\frac{5}{2}^-$ and $\frac{9}{2}^-$ members of the $\frac{1}{2}[541]$ g.s.b., are $\frac{5}{2}^-$, $\frac{7}{2}^{\pm}$, and $\frac{9}{2}^-$. In the vicinity of the Fermi level for $Z=77$, the only proton states meeting this requirement are the $\frac{9}{2}^-[514]$ and $\frac{7}{2}^+[404]$ configurations, as predicted by shell-model calculations using a quadrupole deformation β_2 of the order of 0.2, as estimated from the measured quadrupole moment $Q_0=6.0\pm0.2$ e b of the g.s.b. of ^{181}Ir (Ref. [5]). The deduced value of $g_K=1.19\pm0.11$ for the rotational band built on the 366.2-keV isomeric state compares well with the values of 1.15 and 1.29 predicted for the $\frac{9}{2}^-[514]$ state by the Woods-Saxon and the Nilsson models, respectively, while it clearly differs from the corresponding values of 0.58 and 0.63 calculated for the $\frac{7}{2}^+[404]$ proton state (see Sec. IV A). Therefore, we propose the $\frac{9}{2}^-[514]$ Nilsson quantum number for this isomeric state.

The $\frac{9}{2}^-[514]$ state was also observed [13] in ^{181}Ir. It populates the $\frac{9}{2}^-$, $\frac{7}{2}^-$, and $\frac{5}{2}^-$ states, assumed to be members of the $\frac{1}{2}^-[541]$ rotational band. If we assume $E2$ multipolarity of the populating transitions—preferred over $M1$ multipolarity by forbidden character ($\Delta K=4$) of these transitions—the reduced intensity ratios are 0.056:0.93:0.012, in good agreement with the respective ratios of 0.065:0.93:0.001 observed in the decay of the 366.2-keV isomer in ^{181}Ir and, thus, supporting the $\frac{7}{2}^-$ assignment for the 310.1-keV level (Sec. III B). In the latter case the intensity of the postulated, but unobserved 56.1-keV transition was assumed to be equal to the sum of the intensities of the 285.4- and 310.1-keV transitions depopulating the 310.1-keV level in the delayed coincidence spectrum gated by transitions feeding the isomeric level.

The coincidence relations establish the strongly coupled rotational band built on the $\frac{9}{2}^-[514]$ isomeric state up to a maximum spin of $(\frac{33}{2})$. For most transitions, their $\Delta I=1$ or $\Delta I=2$ character can be deduced from the angular distribution data. However, the lowest transitions, viz., the 288.4-keV crossover transition and the 117.4-keV cascade transition, are not well resolved from other transitions in the angular distribution spectra and, therefore, their multipolarity remains unestablished. The total internal conversion coefficient of the 117.4-keV transition deduced from coincidence intensity balance, $\alpha_{tot}=6.8\pm2.0$, is somewhat higher than the value of 4.1 expected for the $M1$ multipolarity suggested in Ref. [8] for this transition, but the possibility of a systematic error in the low-energy part of the efficiency curve in our coincidence experiment cannot be completely excluded. This transition is contaminated in the coincidence data too by the strong 118.2-keV γ ray from the Coulomb excitation of the ^{169}Tm target and the 118.0-keV γ ray from ^{181}Os radioactive decay, both of which have delayed components as well.

Three additional levels decaying to the $\frac{9}{2}^-[514]$ rotational band have been established from the coincidence data. The angular distribution of the 625.4-keV transition deexciting the 1882.1-keV level indicates its mixed $M1/E2$, $\Delta I=1$ character and, consequently, a spin and parity of $\frac{21}{2}^-$ is proposed for the parent level. However, an absence of observed transitions to the $\frac{23}{2}^-$, $\frac{21}{2}^-$, and $\frac{17}{2}^-$ members of the $\frac{9}{2}^-[514]$ rotational band is difficult to explain. The deexcitation pattern allows $\frac{17}{2}$ with either parity or $\frac{19}{2}^-$ spin and parity assignment for both of the proposed 1955.9- and 1961.0-keV levels.

Other states populating these three additional levels will be discussed in the next subsection.

D. The high spin isomer

The time distribution spectra of transitions in the $\frac{9}{2}^-[514]$ rotational band below the $\frac{19}{2}^-$ level and the 625.4-keV transition feeding this level have delayed components with a mean value of half-life of 22 ± 4 ns (Sec. II C), indicating an existence of an isomer decaying into this band. A detailed study of the prompt-delayed and prompt-prompt coincidence spectra reveals a strongly coupled band built on the isomeric state (Fig. 3). The decay scheme of the isomer could not be determined unambiguously because several of the involved transitions are either doublets (mixed with radioactivity or $3n$ reaction channel transitions) or weak. The isomer decays to the 1882.1-, 1955.9-, and 1961.0-keV levels, and possibly, to other unidentified levels. In addition to the transitions depopulating identified levels, several other transitions not placed in the level scheme (318.1, 332.0, 376.8, 380.2, and 704.4 keV) are seen in the delayed coincidence spectra started by transitions above the isomer. All of them are seen also in the delayed 340.1-keV coincidence gate suggesting that all cascades of transitions depopulating the isomer feed exclusively the $\frac{9}{2}^-[514]$ rotational band. However, different ratios of intensities of transitions following the decay of the isomer are observed in delayed coincidence spectra gated by different transitions above the isomer. The delayed 117.2- and 318.1-keV transitions are relatively much stronger in the 236.1 and 157.4-keV coincidence gates, respectively. The delayed 380.2-, 625.4-, and 914.9-keV transitions are relatively stronger in 157.4- and 190.5-keV coincidence gates while the delayed 376.8, 386- (probably a doublet), and 919.9-keV transitions are relatively stronger in the 215.4- and 236.1-keV coincidence gates. These results imply a rather complex, fragmented decay of the isomer with some transitions deexciting states above the isomer bypassing the isomeric level or, possibly, the existence of two closelying isomeric states, as observed in ^{179}Re (Ref. [15]), ^{181}Re (Ref. [16]), and ^{185}Ir (Ref. [2]). Consequently, only a lower limit of 1961.0 keV can be deduced for the excitation energy of the isomer. For the same reason, the spin

of the isomer cannot be determined directly. Feeding of the 1882.1-, 1955.9-, and 1961.0-keV levels implies that the spin of the isomer has a value higher than $\frac{19}{2}$.

Excluding the possibility of a transition probability faster than the Weisskopf estimate, the short half-life of 22 ns allows only an $E1$ or $M1$ multipolarity for an unobserved transition with an energy lower than about 100 keV. If this transition feeds the 1882.1-keV ($\frac{21}{2}^-$) level directly, the isomer would have an excitation energy lower than 1980 keV and spin not higher than $\frac{23}{2}$. In that event, the 1961.0-keV level could be the isomeric one. Excluding the possibility of an unobserved deexciting transition, partial half-lives of the 919.9- and 1123.0-keV transitions deexciting this level allow for $E1$, $M1$, $E2$, and $M2$ multipolarities of both of these transitions, and also $E3$ for the latter transition, limiting the possible spin of the isomer to values not higher than $\frac{21}{2}$; higher spin values are possible only if the isomer has an energy higher than 1961 keV *and* if one assumes a fragmented decay through some intermediate levels.

E. The $\frac{5}{2}^+[402]$ rotational band

The strongly coupled band is seen in the delayed coincidence gate set on the 289.2-keV transition depopulating the isomeric ($\tau_{1/2}=0.33^{+0.10}_{-0.06}$ μs) level. This band is populated in the ^{16}O-induced reaction with only half as much intensity as the $\frac{9}{2}^-[514]$ rotational band suggesting that the spin of the isomeric bandhead is lower than $\frac{9}{2}$. Therefore, one may conclude that the 289.2-keV isomeric transition feeds the $\frac{5}{2}^-$ ground state. No other transitions deexciting this isomer were found. The transition intensity balance for the 289.2-keV state leads to the calculated value of $\alpha_{\rm tot}=-0.2\pm0.2$ for the total internal conversion coefficient of the depopulating 289.2-keV transition, thus limiting the choice of its multipolarity, within 2 standard deviations, to $E1$ (calculated [14] $\alpha^{\rm th}_{\rm tot}=0.028$) or $E2$ ($\alpha^{\rm th}_{\rm tot}=0.107$) with a small $M1$ ($\alpha^{\rm th}_{\rm tot}=0.325$) admixture. Three $\frac{1}{2}^-$ levels, at about 110, 117 (Ref. [7]), and 135.3 keV (Ref. [17]), have been observed in ^{181}Ir, ^{183}Ir, and ^{185}Ir, respectively, and interpreted as the $\frac{1}{2}^-\frac{1}{2}[541]$ intrinsic state. This state is expected from our calculation (Sec. IV B) to be at 100–170 keV above the $\frac{5}{2}^-$ ground state. Lack of any observed transitions from the 289.2-keV state to the expected $\frac{1}{2}^-$ state and the $\frac{9}{2}^-$ state at 24.7 keV favors a $\frac{5}{2}^+$ assignment for the 289.2-keV isomer, in disagreement with the $\frac{3}{2}^+$ assignment proposed in Ref. [7]. In both cases, the 289.2-keV transition would have an $E1$ multipolarity and a hindrance factor relative to the Weisskopf estimate of 3.9×10^7; comparable hindrance factors of 1.6×10^8 and 3.7×10^7 have been found [18,19] in the $N=104$ isotones ^{179}Re and ^{177}Ta, respectively, for the $E1$ transitions between the $\frac{5}{2}^+[402]$ and $\frac{5}{2}^-\frac{1}{2}[541]$ states. In contrast, the hindrance factors for the $E1$ transitions from the other low-K proton orbitals ($\frac{1}{2}^+[400]$ and $\frac{3}{2}^+[402]$) observed in the heavier Ir nuclei [2–4], to the $\frac{1}{2}^-[541]$ rotational band are 2–3 orders of magnitude smaller. The deduced value of $g_K=1.50\pm0.12$ for the rotational band built on the 289.2-keV isomeric state (see Sec. IV A), agrees very well with the value of 1.57 calcuated for the $\frac{5}{2}^+[402]$ state within the framework of the Nilsson model with the deformation parameters $\varepsilon_2=0.225$ and $\varepsilon_4=0.037$ while strongly differing from the values of 3.38 and 0.17 calculated for their $\frac{1}{2}^+[402]$ and $\frac{3}{2}^+[402]$ proton states, respectively. Consequently, the $\frac{5}{2}^+[402]$ Nilsson quantum number is proposed for this isomeric state. The rotational band built on this state had been observed, but not identified properly at the time, in the ^{185}Ir nucleus [2] and, recently, also in ^{183}Ir (Ref. [20]).

The coincidence and sum relations between assumed $\Delta I=1$ and $\Delta I=2$ transitions seen in the delayed gate set on the 289.2-keV transition (see Fig. 2, upper part) establish the strongly coupled rotational band built on the $\frac{5}{2}^+[402]$ isomeric state up to a maximum spin of ($\frac{29}{2}$).

IV. DISCUSSION

A. Reduced transition probabilities and g factors

Model-independent reduced transition probabilities ratios can be calculated [21–24] as

$$\frac{B(M1,I\to I-1)}{B(E2,I\to I-2)} = 0.6967\frac{E_\gamma^5(I\to I-2)}{E_\gamma^3(I\to I-1)\lambda(1+\delta^2)}\,\mu_N^2/e^2{\rm b}^2 \quad (1)$$

and

$$\frac{B(E2,I\to I-1)}{B(E2,I\to I-2)}=\frac{E_\gamma^5(I\to I-2)\delta^2}{E_\gamma^5(I\to I-1)\lambda(1+\delta^2)}\,, \quad (2)$$

where the experimental branching ratio, $\lambda=I_\gamma(I\to I-2)/I_\gamma(I\to I-1)$, and the square of the dipole-quadrupole mixing ratio,

$$\delta^2=I_\gamma(E2,I\to I-1)/I_\gamma(M1,I\to I-1)\,,$$

are determined [9] from the experimental angular distribution coefficients A_2 and A_4 (Table I), with values of σ/I deduced from angular distributions of stretched $E2$ transition in the yrast cascade. The transition energies in Eqs. (1) and (2) are given in MeV.

In the framework of the rotational model [10], a comparison of the crossover to cascade branching ratios λ and the mixing ratios δ for $\Delta I=\pm1$ transitions in a rotational band provide information on the g factors in a rotational band. The quantity g_K-g_R is a constant for all the rotational states in an unperturbed band and, by comparison to the theoretical values derived from Nilsson model calculations, provides information about internal structure of the appropriate Nilsson orbitals. Assuming that branching ratio λ and mixing ratio δ are known, the following quantities can be calculated:

$$\frac{g_K-g_R}{Q_1}=\frac{0.933E_\gamma(I\to I-1)}{(I^2-1)^{1/2}\delta}\,(e\,{\rm b})^{-1}\,, \quad (3)$$

$$\frac{g_K-g_R}{Q_0}=\left[\frac{0.8709\,A(I,K)E_\gamma^5(I\to I-2)}{(I^2-1)\lambda(1+\delta^2)E_\gamma^3(I\to I-1)}\right]^{1/2}(e\,\mathrm{b})^{-1}, \tag{4}$$

with

$$A(I,K)=[\langle IK20|I-2\,K\rangle/\langle IK20|I-1\,K\rangle]^2$$
$$=(I+1)(I-1+K)(I-1-K)/[2K^2(2I-1)]$$

and where transition energies are given in MeV. The sign of $(g_K-g_R)/Q_0$ is taken to be the same as the sign of δ. In the framework of the rotational model, the quadrupole moments Q_0 and Q_1, defined as

$$eQ_0=[(16\pi/5)B(E2,I\to I-2)/\langle IK20|I-2K\rangle]^{1/2}, \tag{5a}$$

$$eQ_1=[(16\pi/5)B(E2,I\to I-1)/\langle IK20|I-1K\rangle]^{1/2}, \tag{5b}$$

are equal for an unperturbed rotational band and cannot be determined only from λ and δ.

Even when it is not possible to extract the values of δ experimentally, it is still possible to get this value from the rotational formula:

$$\frac{1}{\delta^2}=\frac{A(I,K)E_\gamma^5(I\to I-2)}{\lambda E_\gamma^5(I\to I-1)}\left[\frac{Q_0}{Q_1}\right]^2-1 \tag{6}$$

with $A(I,K)$, Q_0, and Q_1 as defined above. In most cases of interest, δ^2 is small and, therefore, the additional uncertainty introduced by the use of the calculated value of δ^2 does not introduce large uncertainties into the values of $B(M1,I\to I-1)/B(E2,I\to I-2)$ and $(g_K-g_R)/Q_0$ [see Eqs. (1) and (4)], while it may affect significantly the values of $B(E2,I\to I-1)/B(E2,I\to I-2)$ and $(g_K-g_R)/Q_1$ [Eqs. (2) and (3)].

The values of quantities defined above, as determined from the experimental data (Table I), are given in Tables II and III. For both rotational bands (based on the $\frac{9}{2}^-[514]$ and $\frac{5}{2}^+[402]$ orbitals), the respective quantities $(g_K-g_R)/Q_0$ remain constant within the experimental errors, validating the use of the rotational model. This is further corroborated by a value (expected from the rotational model to be close to 1.0) of the ratio

TABLE II. Mixing ratios, branching ratios, reduced transition probabilities ratios, and deduced $(g_K-g_R)/Q_0$ and $(g_K-g_R)/Q_1$ values.

I_i	λ	δ	$\frac{B(M1,I\to I-1)}{B(E2,I\to I-2)}$	$\frac{B(E2,I\to I-1)}{B(E2,I\to I-2)}$	$\frac{g_K-g_R}{Q_0}$	$\frac{g_K-g_R}{Q_1}$
			$\frac{9}{2}^-[514]$ rotational band			
$\frac{13}{2}$	0.12(2)	0.211(26)	2.3(4)	5.0(21)	0.103(10)	0.118(15)
$\frac{15}{2}$	0.38(5)	0.230(18)	1.56(20)	3.5(10)	0.108(7)	0.100(8)
$\frac{17}{2}$	0.78(9)	0.226(25)	0.88(10)	1.6(5)	0.090(6)	0.099(11)
$\frac{19}{2}$	0.75(10)		1.15(15)[a]		0.110(8)[a]	
$\frac{21}{2}$	1.16(17)		0.83(13)[a]		0.097(8)[a]	
$\frac{23}{2}$	1.23(17)		0.91(13)[a]		0.105(8)[a]	
$\frac{25}{2}$	1.8(3)		0.68(14)[a]		0.092(9)[a]	
$\frac{27}{2}$	2.6(8)		0.51(20)[a]		0.081(15)[a]	
$\frac{29}{2}$	2.3(6)		0.62(16)[a]		0.091(12)[a]	
$\frac{31}{2}$	1.2(3)		1.3(3)[a]		0.134(16)[a]	
$\frac{33}{2}$	2.7(9)		0.6(2)[a]		0.092(17)[a]	
				Weighted mean value	0.100(4)	
			$\frac{5}{2}^+[402]$ rotational band			
$\frac{9}{2}$	0.24(7)		0.9(3)[a]		0.137(22)[a]	
$\frac{11}{2}$	0.53(9)	0.04(4)	0.65(12)	0.06^{+29}_{-6}	0.142(13)	$0.65^{+\infty}_{-35}$
$\frac{13}{2}$	0.60(10)		0.79(14)[a]		0.170(15)[a]	
$\frac{15}{2}$	0.86(14)		0.71(12)[a]		0.167(14)[a]	
$\frac{17}{2}$	1.3(2)		0.57(11)[a]		0.154(14)[a]	
$\frac{19}{2}$	1.5(3)		0.60(12)[a]		0.161(15)[a]	
$\frac{21}{2}$	2.0(5)		0.51(12)[a]		0.150(18)[a]	
$\frac{23}{2}$	2.2(6)		0.51(15)[a]		0.152(22)[a]	
$\frac{25}{2}$	3.2(9)		0.38(13)[a]		0.132(21)[a]	
$\frac{27}{2}$	3.2(10)		0.42(16)[a]		0.139(25)[a]	
$\frac{29}{2}$	3.4(13)		0.44(20)[a]		0.14(3)[a]	
				Weighted mean value	0.152(6)	

[a]Calculated with δ^2 value given by Eq. (6) assuming $Q_1/Q_0=1$, see text.

TABLE III. Mixing ratios, branching ratios, and reduced transition probabilities ratios of intraband to interband transitions in the $\frac{3}{2}^-[532]$ and $\frac{1}{2}^-[541]$ bands. Th. (EAR), values predicted by extended asymmetric rotor model; and Th. ($N+C$), values predicted by Nilsson model with Coriolis coupling.

$\frac{I\to I-1}{I\to I-2}$	$\frac{I_\gamma(I\to I-1)}{I_\gamma(I\to I-2)}$	$\delta_{I\to I-1}$	$\frac{B(M1,I\to I-1)}{B(E2,I\to I-2)}$	$\frac{B(E2,I\to I-1)}{B(E2,I\to I-2)}$
$\frac{\frac{15}{2}\to\frac{13}{2}}{\frac{15}{2}\to\frac{11}{2}}$	≥ 5.8	$-0.16(7)$	≥ 0.057	≥ 0.006
		or -3.6^{+7}_{-12}	or ≥ 0.004	or ≥ 0.22
Th. (EAR)	25.0	-0.46	0.210	0.171
Th. ($N+C$)	9.2	-0.45	0.077	0.062
$\frac{\frac{19}{2}\to\frac{17}{2}}{\frac{19}{2}\to\frac{15}{2}}$	≥ 2.5	$-0.22(8)$	≥ 0.074	≥ 0.011
		or -3.0^{+6}_{-9}	or ≥ 0.008	or ≥ 0.21
Th.(EAR)	7.0	-0.49	0.153	0.112
Th. ($N+C$)	3.1	-0.41	0.080	0.040
$\frac{\frac{23}{2}\to\frac{21}{2}}{\frac{23}{2}\to\frac{19}{2}}$	1.4(4)	$-0.27(12)$	0.077(24)	0.014^{+24}_{-10}
		or -2.8^{+8}_{-12}	or 0.009^{+14}_{-6}	or 0.18(8)
Th. (EAR)	2.4	-0.49	0.118	0.070
Th. ($N+C$)	1.6	-0.37	0.082	0.028
$\frac{\frac{27}{2}\to\frac{25}{2}}{\frac{27}{2}\to\frac{23}{2}}$	0.7(2)	0.3(1)[a]	0.07^{+3}_{-2}	0.013^{+17}_{-8}
		or 4.8^{+32a}_{-15}	or 0.003^{+5}_{-2}	or 0.015(5)
Th. (EAR)	1.13	-0.45	0.098	0.044
Th.($N+C$)	0.93	-0.35	0.083	0.023

[a]The angular distribution coefficients for the 810.2-keV, $\frac{27}{2}^-\to\frac{25}{2}^-$ transition are inconsistent with its deduced $\Delta I=-1$ character, see text.

$Q_1/Q_0=0.96\pm0.11$ deduced from the branching ratios of transitions deexciting the $\frac{13}{2}^-$, $\frac{15}{2}^-$, and $\frac{17}{2}^-$ members of the $\frac{9}{2}^-[514]$ rotational band. The $B(M1,I\to I-1)/B(E2,I\to I-2)$ ratios for both $\frac{9}{2}^-[514]$ and $\frac{5}{2}^+[402]$ bands show slight decrease with spin and a hint of staggering for lower spin values.

B. High spin isomer

Isomeric states with spin parity of 7^- and with half-lives of the order of 20 ns are observed in the even-even $N=104$ isotones [25–28] at an excitation energy of 1.74–1.96 MeV. In the two neighboring isotones of ^{181}Ir, the ^{180}Os and ^{182}Pt nuclei, the excitation energies of 7^- states differ only by 27 keV and the moments of inertia of the rotational bands built on these states are nearly identical for several lowest transitions. It supports the conclusion [27] that these states are dominated by a two-quasineutron configuration. They deexcite predominantly by low-energy $E1$ transitions to presumed two-quasiparticle 6^+ states (which may also be isomeric states, as in the case of ^{178}W), but the decay pattern becomes more complex with increasing Z. Isomers with similar excitation energy and half-life have been observed in the odd proton $N=104$ and 106 Re isotopes [15,16]; these decay through some intermediate states into the $\frac{9}{2}^-[514]$ rotational band. A rotational band at 1.74 MeV, with similar level spacings and deexciting finally into the $\frac{9}{2}^-[514]$ state, has recently been observed [8] in ^{183}Ir also, although no half-life was reported for the $(\frac{21}{2}^+)$ bandhead.

The observed high spin isomer at $E\geq 1.96$ MeV decaying to the $\frac{9}{2}^-[514]$ rotational band in ^{181}Ir fits nicely into these systematics. Its half life (22 ns) and excitation energy closely match the corresponding values for the 7^- isomer in ^{180}Os. Moreover, the level spacings above the isomer in ^{181}Ir are surprisingly close to the rotational level spacings above the 8^- states in the corresponding bands built on the 7^- states in ^{180}Os and ^{182}Pt, although it is difficult to explain why no transition corresponding to the $8^-\to 7^-$ transitions is observed. Nonetheless, it is reasonable to assume that the isomer in ^{181}Ir arises from a coupling of the odd proton particle to the 7^- isomeric state in ^{180}Os core or the proton hole to the 7^- state in ^{182}Pt. On the basis of the analogies discussed above, one may expect in ^{181}Ir the occurrence of an isomeric $\{7^-\otimes\frac{9}{2}^-[514]\}_{23/2^+}$ configuration, decaying through the $\{6^+\otimes\frac{9}{2}^-[514]\}_{21/2^-}$ configuration to the $\frac{9}{2}^-[514]$ rotational band. The fact that the strongest decay path of the isomer (see Sec. III D) passes through the $(\frac{21}{2}^-)$, 1882.1-keV state supports this suggestion. The other strong decay path of the isomer in ^{180}Os and the 7^- state in ^{180}Pt (Ref. [28]) goes through the 5^- state and, therefore, one may suspect that one of the unplaced transitions observed in the decay of the isomer in ^{181}Ir leads to a state with $\{5^-\otimes\frac{9}{2}^-[514]\}_{19/2^+}$ configuration. Another possible decay mode of the isomer in ^{181}Ir would be to members of the rotational band built on the $\frac{11}{2}^-[505]$ proton state

which is expected, on the basis of systematics and Woods-Saxon model calculations, at 1.2±0.2 MeV above the ground state. If so, one of the $(\frac{17}{2}, \frac{19}{2}^-)$ states at 1955.9 and 1961.0 keV could be the $\frac{17}{2}^-$ member of this rotational band, expected [2,3] at approximately 900 keV above the $\frac{11}{2}^-[505]$ bandhead.

Other possible configurations of the isomeric states are $\{7^- \otimes \frac{1}{2}^-[541]\}_{15/2^+}$ and $\{7^- \otimes \frac{5}{2}^+[402]\}_{19/2^-}$. The relative excitation energies of these states depend not only on single-quasiparticle energies but also on residual interactions. The presence of these states could explain the complicated deexcitation pattern of the isomer as discussed in Sec. III D.

A value of $|(g_K - g_R)/Q| = 0.03 \pm 0.01$ has been extracted from the branching ratios of $\Delta I = 1$ and $\Delta I = 2$ transitions in the rotational band associated with the isomer, using Eqs. (4) and (6), with $Q_0 = Q_1$; the quoted error includes the uncertainty in K. This value is only a little higher than the corresponding value of 0.017±0.006 for the band associated with the 7^- isomer in ^{180}Os (Ref. [27]). Using an estimated value of $Q_0 = 10 \pm 1$ e b and $g_R = 0.41 \pm 0.07$, the experimental g_K factor of this band has been deduced to be $g_K = 0.7 \pm 0.1$ or 0.08 ± 0.10, for $\delta > 0$ or $\delta < 0$, respectively. The angular distribution of the 157.4-keV transition slightly favors the former value, in good agreement with the value obtained [15] for the high spin isomer in ^{179}Re.

The g_K factors calculated in the framework of the Nilsson model for three-quasiparticle configurations with total spin $I \geq \frac{15}{2}$ and involving the lowest-lying quasineutron and quasiproton states range from −0.2 to 0.5 for $(\nu^2\pi)$ configurations (the lowest values are obtained when the $\pi\frac{1}{2}^-[541]$ configuration is involved), while they are close to 1.3 for the (π^3) configurations, excluding the latter possibility for the isomer in ^{181}Ir. The coupling of the predominantly two-quasineutron 7^- state in ^{180}Os [experimental $g_K = 0.17 \pm 0.05$ (Ref. [27])] to $\frac{1}{2}^-[541]$, $\frac{5}{2}^+[402]$, or $\frac{9}{2}^-[514]$ proton states would result in g_K values of the resultant $(\nu^2\pi)$ configuration of about 0.2, 0.5, and 0.6, respectively. The experimental value of $g_K = 0.7 \pm 0.1$ deduced for the high spin isomer in ^{181}Ir (assuming $\delta > 0$) thus favors the $(\nu^2\pi)$ configuration involving a $\frac{9}{2}^-[514]$ proton, with a possible admixture of (π^3) proton configurations; the second possibility, $g_K = 0.08 \pm 0.10$ (deduced with $\delta < 0$), would indicate a configuration involving a $\frac{1}{2}^-[541]$ proton instead. The latter seems to be excluded by the deduced spin of the isomer ($\geq \frac{19}{2}$), however. It follows that knowledge of the sign of dipole-quadrupole mixing ratios, δ, in the rotational band built on the high spin isomer in ^{181}Ir is essential for better elucidation of its structure.

The relatively short half-life for $\Delta K \geq 5$ and the fragmented decay of the isomer are in agreement with the general tendency towards lower hindrance factors and rising complexity of the decay modes of high spin isomers, with increasing Z, in the Yb-Pt nuclei [27–30]. The observed breakdown of the K selection rule may result from a triaxial deformation or, at least, a softness toward dynamical γ distortions.

C. Axial and nonaxial model calculations for the $h_{9/2}$ level system

1. *Nilsson model with Coriolis interaction* ($N + C$)

In order to describe rotational bands built on low-K, high-j orbitals, the Coriolis interaction has to be taken into account. An analysis of the $h_{9/2}$ proton bands in the framework of the Nilsson model [31] with hexadecapole deformation, pairing interaction, and Coriolis coupling and also including the $f_{7/2}$ subshell was performed previously for odd-A $^{185-189}$Ir isotopes [2,3] using the computer code CORIOLIS [32]. The same method was used for analysis of the yrast and yrare bands built on the $h_{9/2}$ orbital in ^{181}Ir. All single-particle states originating from this orbital as well as the two lowest states from the $f_{7/2}$ orbital, expected to lie close to the Fermi surface for $Z = 77$, were included into the diagonalized matrix. The calculated level energies were fitted to the experimental ones with the following free parameters: the Fermi energy λ, attenuation coefficient of the Coriolis matrix elements α, parameter of inertia $\hbar^2/(2\mathcal{J}_0)$ and a parameter, B, describing changes of inertia parameter with spin according to the formula

$$\frac{\hbar^2}{2\mathcal{J}} = \frac{\hbar^2}{2\mathcal{J}_0} + BI(I+1) \ . \tag{7}$$

In addition, the decoupling parameter, a, of the $\frac{1}{2}^-[541]$ state and the energy ε_{532} of the $\frac{3}{2}^-[532]$ state were allowed to vary. All other quantities were calculated from the Nilsson model for several sets of deformation parameters $(\varepsilon_2, \varepsilon_4)$. The quality of the resulting fits, with energy of the $\frac{3}{2}^-[532]$ state taken as a free parameter, is not very sensitive to the choice of the deformation parameters. The best fit, however, was obtained with values $\varepsilon_2 = 0.265$ and $\varepsilon_4 = 0.037$ for which ε_{532} coincides with the one obtained from Nilsson model. In this case, the quality of level-energy fit was $\chi^2 = 9.7$ keV, where

$$\chi^2 = \left[\sum_i (E_i^{\exp} - E_i^{\text{calc}})^2 / n \right]^{1/2} , \tag{8}$$

and n is the number of experimental levels. Thirteen negative-parity yrast and yrare levels below the backbending region were included in the fitting procedure. The results are presented in Table IV. As in the case of ^{185}Ir, the results of the calculation show that the main components of the wave function are $\frac{1}{2}^-[541]$ for the ground-state band and $\frac{3}{2}^-[532]$ for the yrare band built on the $\frac{7}{2}^-$ state at 310.1 keV. No satisfactory fit can be obtained under the assumption that the observed yrare band is an unfavored sequence of the $\frac{1}{2}^-[541]$ decoupled rotational band. The fitted value of the decoupling parameter $a = 3.34$ is considerably lower than $a_{\text{Nilss}} = 4.18$ calculated from the Nilsson model with deformation parameters $\varepsilon_2 = 0.265$ and $\varepsilon_4 = 0.037$. However, when only the low spin levels are fitted, a "best-fit" value of $a = 3.8$ is obtained; lowering of the hexadecapole parameter by 0.04 in Nilsson model calculations, on the other hand, results in a decrease in the calculated value of the decoupling parameter a by 0.5.

TABLE IV. The $h_{9/2}$ negative-parity states in ^{181}Ir from the EAR and $N+C$ model calculations. The best-fit parameters are $\lambda=6.034\hbar\omega_0$, $\alpha=1.00$, $\hbar^2/2\mathcal{I}=19.8$ keV, $B=-16.2$ eV, $a=3.34$, and $\varepsilon_{532}=6.180\hbar\omega_0$ for the Coriolis model, and $\tilde{\lambda}=0.426$, $\alpha=0.861$, $\hbar^2/2\mathcal{I}=17.9$ keV, and $B=-9.6$ eV for the EAR model.

	Level energy (keV)			Amplitude of wave functions ($N+C$)						
Spin	Expt.	EAR	$N+C$	$\frac{1}{2}$[541]	$\frac{1}{2}$[530]	$\frac{3}{2}$[521]	$\frac{3}{2}$[532]	$\frac{5}{2}$[523]	$\frac{7}{2}$[514]	$\frac{9}{2}$[505]
$\frac{1}{2}$		172.2	77.4	0.999	−0.052					
$\frac{3}{2}$		254.1	228.5	0.833	0.162	0.024	0.528			
$\frac{5}{2}$	0.0	6.7	−12.2	0.910	−0.088	0.007	0.401	0.053		
$\frac{7}{2}$	310.1	305.2	303.2	0.663	0.269	0.065	0.676	0.163	0.012	
$\frac{9}{2}$	24.7	24.7	35.9	0.865	−0.100	0.008	0.479	0.111	0.011	0.000
$\frac{11}{2}$	499.0	500.9	492.1	0.586	0.338	0.102	0.689	0.237	0.032	0.001
$\frac{13}{2}$	212.5	210.8	228.3	0.837	−0.104	0.010	0.515	0.151	0.021	0.001
$\frac{15}{2}$	814.8	820.2	806.9	0.541	0.380	0.133	0.680	0.283	0.051	0.004
$\frac{17}{2}$	548.1	548.3	556.0	0.818	−0.106	0.011	0.535	0.179	0.031	0.002
$\frac{19}{2}$	1244.2	1241.8	1238.8	0.512	0.408	0.156	0.668	0.312	0.066	0.006
$\frac{21}{2}$	1003.9	1007.4	1001.9	0.804	−0.107	0.012	0.548	0.201	0.039	0.004
$\frac{23}{2}$	1762.6	1758.6	1769.7	0.492	0.425	0.173	0.657	0.332	0.078	0.008
$\frac{25}{2}$	1549.6	1552.3	1542.1	0.795	−0.107	0.013	0.556	0.216	0.046	0.005
$\frac{27}{2}$	2359.8	2359.9	2373.0	0.479	0.437	0.185	0.648	0.345	0.087	0.010
$\frac{29}{2}$	2154.4	2154.4	2145.8	0.787	−0.107	0.014	0.561	0.227	0.051	0.006

The calculated wave functions for states of both rotational bands were used for calculating the mixing ratios, and reduced transition probabilities in both bands. The results are compared with the experimental data in Tables III and IV and will be discussed later (see Sec. IV C 3).

2. *Extended asymmetric rotor model (EAR)*

The Coriolis calculations described earlier had assumed an axially symmetric shape for the nucleus and had treated the nonaxiality only as a perturbation. An alternative approach, viz., assuming a rigid nonaxial shape for the nuclear potential, has also been successfully applied to a number of odd-A Ir nuclei for the level systems built on the $h_{9/2}$ and $h_{11/2}$ subshell [2,3,33]. However, the original model [33]—assuming an odd nucleon coupled to a triaxial, rotating, rigid core—does not take into account some well-established empirical effects, viz., the attenuation of the strength of the Coriolis interaction in comparison with its theoretical estimates; the differences in the moments of inertia of the odd-A nucleus and the even-even core nucleus caused by polarization of the even core by the odd particle and the changes in the pairing force due to the blocking effect. Therefore, an extended version of triaxial model (EAR) was developed [34] in which these effects are included. In this approach, the attenuation coefficient α, the inertia parameter $\hbar^2/2\mathcal{I}_0$, as well as the softness parameter B [see Eq. (7)], and the Fermi energy λ, are taken as free parameters. The values of the free parameters were adjusted by a least-squares fit to the experimental level energies. The calculations have been done for several values of the nonaxial deformation parameter γ and the best fit was achieved for the value of $\gamma=15.3°$ which is very close to 14.9°, the mean value of this parameter obtained from the experimental energies of $2^+_{\text{g.s.b.}}$ and 2^+_γ, 4^+_γ, and 6^+_γ levels, respectively, in the ^{180}Os core nucleus using the recipe given in Ref. [33]. The resulting best-fit parameters for the $h_{9/2}$ proton systems in the odd-A $^{181-189}$Ir isotopes are given in Table V together with several related values; in all cases, only the levels below the backbending region were included in the fitting procedure.

The similar values of parameter γ obtained from best fit for the $\pi h_{9/2}$ systems in odd-A iridium isotopes and those obtained, as described above, for the corresponding Os cores (Table V), as well as the sensitivity of the fitted level energies to this parameter, emphasize the significance of the γ asymmetry and, particularly, the importance of the coupling of the odd particle also to the states of the $K=2$ rotational band (so-called γ-vibrational band). In addition, it seems to justify a physical meaning for the fitted γ values.

Although total-energy calculations in the (β_2,γ) plane do not confirm values of stable γ deformations for the ground state of Os isotopes as large as $\sim 15°$ (see, e.g., Ref. [27] where $\gamma=-6°$ was obtained for low spin states of the g.s.b. in ^{180}Os), they do indicate a considerable softness of these nuclei toward γ deformation. The low-lying 2^+_2 state should then be understood as a dynamical γ-vibrational state rather than as a state resulting from rotation around the second symmetry axis; the γ values derived above would thus be a measure of the γ stiffness of nucleus rather than indicating a stable γ deformation. Even so, the rigid rotor plus particle approach discussed above seems to be an efficient and successful way to take into account rotation-γ-vibration coupling in these nuclei (see also the next section).

3. *Reduced transition probabilities and comparison of the models*

The quality of the EAR fit for 13 experimental levels of the $h_{9/2}$ system in ^{181}Ir ($\chi^2=3.5$ keV [see Eq. (8)]) is

TABLE V. Systematics of parameters describing the $h_{9/2}$ proton systems in odd-A Ir isotopes in the framework of the extended asymmetric rotor model.

Parameters	^{181}Ir	^{183}Ir[a]	^{185}Ir	^{187}Ir	^{189}Ir
$\tilde{\lambda}$	0.426	0.342 (0.52)	0.350	0.334	0.376
α	0.861	0.802 (0.85)	0.908	0.921	0.956
$\hbar^2/2\mathcal{J}$ (keV)[b]	20.63	15.80 (17.6)	17.39	19.73	22.64
B (eV)	−9.6	−2.7=const	−2.7	−0.6	0.0
β_2	0.248	0.278 (0.27)	0.258	0.247	0.234
$\gamma_{\text{best fit}}$	15.3°	14.6° (16.6°)	13.0°	16.4°	19.2°
$\gamma_{\text{Os core}}$	14.9°	14.6°	13.9°	16.4°	18.9°
N_{lev}	13	7 (7)	21	19[c]	9
Spin range	$\frac{1}{2}-\frac{29}{2}$	$\frac{5}{2}-\frac{25}{2}$	$\frac{1}{2}-\frac{41}{2}$	$\frac{1}{2}-\frac{33}{2}$	$\frac{1}{2}-\frac{21}{2}$
χ^2 (keV)	3.5	4.4 (1.9)	5.1	12.0[c]	7.4

[a]It is difficult to obtain unique fit for ^{183}Ir where only seven experimental levels below backbending anomalies are known and therefore two examples of fit are given.
[b]Calculated from Eq. (9) using best-fit value of $\hbar^2/2\mathcal{J}_0$.
[c]Three fitted levels, namely, $\frac{5}{2}_2$, $\frac{13}{2}_2$, and $\frac{17}{2}_2$ may not belong to the $h_{9/2}$ orbital.

better than that for the axial case ($\chi^2=9.7$ keV). The same conclusion is reached when the EAR model is applied to the $h_{9/2}$ level systems in the other Ir nuclei presented in Table V, as well as in ^{199}Tl (Ref. [34]), demonstrating the relative advantage of the EAR model in describing experimental rotational level energies of this odd-proton system.

The $N+C$ and EAR model wave functions were also used for calculating the properties of the electromagnetic transitions between the levels in ^{181}Ir. The results are presented in Table III. Because the calculated amplitudes of wave functions are explicitly involved, a comparison of the observed and calculated transition probabilities provides, in principle, a more sensitive test of the used models than comparison of the level energies only. Unfortunately, the results for the yrare and yrast bands calculated with $Q_0=6.0$ e b (see Table III) do not permit a definite final conclusion because of large experimental uncertainties in the angular distribution data. The values calculated with the Nilsson model with Coriolis interaction ($N+C$) appear to be closer to the experimental values (if the first choice of δ is accepted) than those calculated within the EAR model; the differences, however, are within error bars in most cases. The same is true when the branching ratio of the transitions deexciting the $\frac{7}{2}^-$ level at 310.1 keV [I_γ(285.4 keV)/I_γ(310.1 keV)=0.86+0.09] is compared with the values of 0.845 and 0.785 calculated with $N+C$ and EAR models, respectively. The differences between reduced transition probabilities calculated from these models increase with decreasing spin so that a comparison of the calculated values with the experimental ones for levels with spin $I \leq \frac{19}{2}$ would be a crucial test of the models.

Nevertheless, such values as the inertia parameter of the rotational bands in the $h_{9/2}$ system, attenuation of the Coriolis interaction, and the softness of the core deduced with the use of both models agree well with each other despite differences in the assumption of axiality. The best-fit value, $\hbar^2/2\mathcal{J}=19.8$ keV, for the inertia parameter obtained in the $N+C$ model agrees well with the value of 20.6 keV obtained in the EAR model with $\gamma=15.3°$ using the formula [33]

$$\frac{\hbar^2}{2\mathcal{J}}=\frac{\hbar^2}{2\mathcal{J}_0}\frac{9-[81-72\sin^2(3\gamma)]^{1/2}}{4\sin^2(3\gamma)} \tag{9}$$

with $\hbar^2/2\mathcal{J}_0=17.9$ keV resulting from the EAR best fit. The agreement is even better when only low spin ($I \leq \frac{15}{2}$) levels are fitted in the $N+C$ model, demonstrating that the moments of inertia of the decoupled bands can be extracted reliably from experimental rotational level spacings using either of these models.

Both models are also in agreement in that the attenuation of the Coriolis interaction in the $h_{9/2}$ system of the odd-A Ir nuclei is weak ($\alpha \approx 0.9$, EAR) or nonexistent ($\alpha \approx 1$, $N+C$). The same conclusion was reached for this system in several other odd-proton transitional nuclei [34] where all the orbitals are close to or above the Fermi level, in contrast with well-deformed rare-earth nuclei for which a considerable attenuation ($\alpha \approx 0.6$) is observed.

Small values of the fitted parameter B for the $\pi h_{9/2}$ systems in odd-A Ir isotopes are another interesting result of both model calculations. The parameter B, defined in Eq. (7), is usually regarded to some degree as a measure of softness of nucleus, although it is also a way to take into account a moderate amount of rotation-vibration mixing. This estimate of the softness of the odd-A Ir nuclei (Table V) does not differ from the well-deformed rare-earth nuclei where $-B/(\hbar^2/2\mathcal{J})$ is of the order of 10^{-3} (see, e.g., Ref. [10]). The respective values of the parameters $\mathcal{J}_1$ in the Harris formula, $\mathcal{J}=\mathcal{J}_0+\mathcal{J}_1\omega^2$, for the odd-$A$ Ir nuclei can be calculated using the equation $\mathcal{J}_1=-4B\mathcal{J}_0^4/\hbar^4$ (with B in MeV) [10]. The resulting values of $\mathcal{J}_1=16\hbar^4/\text{MeV}^3$ and $\mathcal{J}_1=26$ $\hbar^4/\text{MeV}^3$ corresponding to the best-fit values of B from the EAR and $N+C$ models, respectively, for ^{181}Ir, as well as the $\mathcal{J}_1$ values obtained using B values given in Table V for other Ir isotopes, are much smaller than the values for neighboring even-even osmium nuclei which are of the order of $100\hbar^4/\text{MeV}^3$ or higher. They are also

much smaller than the value $\mathcal{J}_1 = 126.9\hbar^4/\text{MeV}^3$ obtained for the ground-state band of ^{181}Ir from the plot of the dynamical moment of inertia $\mathcal{J}^{(2)}$ (the so-called adapted g reference; see Sec. IV D). It is possible that the so-called softness, manifesting itself in the lowering of the energies of the rotational states in comparison to the $I(I+1)$ rotational dependence, originates nearly completely from the Coriolis interaction with members of other rotational bands having the same parity and spin value I, and from γ deformation. It follows that, for the $h_{9/2}$ proton rotational bands below the backbending region in the odd-A iridium nuclei, the alignment of the $i_{13/2}$ neutrons at low rotational frequencies (considered the cause of the high $\mathcal{J}_1$ values in even-even Os isotopes [35]) is small, or even negligible. This statement must be treated with caution, however, since at least part of this effect may be attributed to a stronger Coriolis interaction ($\alpha \approx 0.9$) than that observed in the rare-earth region.

D. Spin alignment and backbending phenomena

An appropriate choice of the reference is crucial for the analysis of the properties of the rotational bands. In the case of ^{181}Ir, the even-even ^{180}Os core parameters do not fulfill the necessary criteria because of the fast and irregular changes in the moment of inertia with rotational frequency even at relatively low rotational frequencies. Therefore, the adapted g reference [36] was used, wherein the $\mathcal{J}_0$ and $\mathcal{J}_1$ reference parameters are determined by plotting the dynamical moment of inertia for the ground-state band

$$\mathcal{J}^{(2)} = \mathcal{J}_0 + 3\omega^2 \mathcal{J}_1 \tag{10}$$

with respect to ω^2 and fitting to the linear part of the plot. Even so, when the interaction with the s band is strong, the extracted values depend on the number of fitting points and the choice of mean spin for the "linear" part. A three-point fit to $\mathcal{J}^{(2)}$ with $I_{\text{mean}} = \frac{17}{2}$ gives $\mathcal{J}_0 = 19.9\hbar^2/\text{MeV}$ and $\mathcal{J}_1 = 126.9\hbar^4/\text{MeV}^3$, resulting in an initial alignment of $i \approx 4.0\hbar$ for the $\frac{1}{2}^-[541]$, $\alpha = +\frac{1}{2}$ signature members. The value of $I_{\text{mean}} = \frac{17}{2}$ was chosen since it gave $i \approx$ const over a wider range of spin values.

The alignments of the bands obtained with $\mathcal{J}_0 = 19.9\hbar^2/\text{MeV}$ and $\mathcal{J}_1 = 126.9\hbar^4/\text{MeV}^3$ are shown in Fig. 4. The ground-state band displays a pronounced crossing at $\hbar\omega = 0.30$ MeV with an alignment gain of $\Delta i = 6.6\hbar$. This value is nearly equal to $6.5\hbar$, the mean value of the sum of the alignments (deduced using the g reference discussed above) of the $\alpha = \pm\frac{1}{2}$ signature members of the $\frac{9}{2}^+[624]$ band in the $N = 103$ and 105 isotopes of Os and Pt; however, it is considerably lower than $\Delta i = 9\hbar$ observed in the neighboring even-even Os isotopes.

In contrast to the $\frac{1}{2}^-[541]$ rotational band, only slight upbendings at $\hbar\omega \approx 0.23$ MeV, evident on plots of $\mathcal{J}^{(2)}$ vs $\hbar\omega$, are observed in both signature members of the rotational bands built on the $\frac{5}{2}^+[402]$ and $\frac{9}{2}^-[514]$ hole configurations. The alignments in both rotational bands rise smoothly with increasing $\hbar\omega$ in relation to the chosen reference parameters, indicating very strong interaction

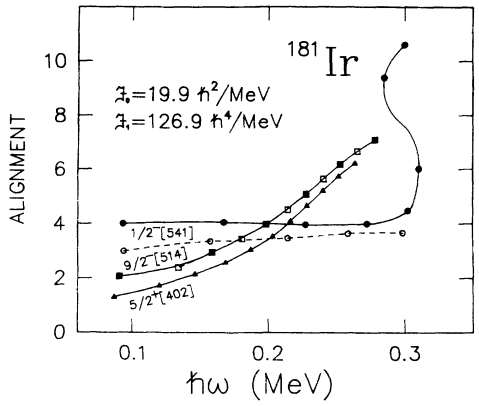

FIG. 4. Plot of the experimental aligned angular moment i of the bands in ^{181}Ir as a function of the rotational frequency $\hbar\omega$.

with the crossing band. Indeed, the $\mathcal{J}_0$ and $\mathcal{J}_1$ parameters—the latter can be used as an indicator of the interaction strength with a crossing band—deduced with the use of Eq. (10) are $24.8\hbar^2/\text{MeV}$ and $340.6\hbar^4/\text{MeV}^3$ for the $\frac{5}{2}^+[402]$ band and $19.6\hbar^2/\text{MeV}$ and $389.9\hbar^4/\text{MeV}^3$ for the $\frac{9}{2}^-[514]$ band, quite different from adapted g reference for the ground-state band. The $\mathcal{J}_1$ parameters so deduced are larger even than the $\mathcal{J}_1$ parameters for g.s.b. in the neighboring even-even Os and Pt isotopes. For both bands, the total alignment gain at the highest observed frequency, $\hbar\omega = 0.28$ MeV, is already about $5\hbar$ with the crossing apparently still continuing. It indicates that a larger ε_2 deformation of these configurations and, perhaps, a different γ deformation, expected when two protons occupy the strongly deformation driving $\frac{1}{2}^-[541]$ state and evident from the moments of inertia (see Sec. IV A), influence their backbending properties. Unfortunately, the highest observed rotational frequencies ($\hbar\omega \approx 0.28$ MeV in both bands) are too low to conclude if the upbending at $\hbar\omega = 0.32$ MeV, with $\Delta i = 4.0\hbar$, observed [28] in ^{182}Pt, which is the core for both hole configurations, occurs in these bands also. A difference of about 70 keV in crossing frequencies and the very different interaction strengths *vis a vis* the crossing band, that distinguish the rotational bands built on the $\frac{5}{2}^+[402]$ and $\frac{9}{2}^-[514]$ hole configurations and the $\frac{1}{2}^-[541]$ band will be discussed in the next section.

The rotational band built on the isomeric state exhibits a continuous increase in alignment from $3.8\hbar$ to $7.1\hbar$ in the observed spin range, quite similar to behavior of the 7^- isomeric band [26,27] in ^{180}Os, thus confirming the suggestion that the isomer in ^{181}Ir arises from the coupling of this core state to an odd proton.

It is difficult to draw a definite conclusion on the reason for the alignment phenomena observed in ^{181}Ir using simply blocking arguments only, since all rotational bands built on the high-j orbitals in the neighboring odd-A nuclei ($i_{13/2}$ neutrons on Os and Pt and $h_{9/2}$ protons in Ir—the best candidates for alignment processes) exhibit a backbending or, at least a strong alignment gain, in the rotational frequency range 0.20–0.34 MeV. Even when the $\frac{1}{2}^-[541]$ configuration (labeled e) is blocked, other

proton crossings (e.g., fg or fh) can, in principle, still appear in the g.s.b. of ^{181}Ir. However, the blocking arguments are valid *only* when all rotational bands under consideration have similar deformations, which is not the case in this mass region.

A pairing-self-consistent cranking (RBCS) calculation [27] for ^{180}Os indicates an $i_{13/2}$ neutron crossing (AB) at 0.26 MeV in the g.s.b., followed by BC and AD crossings at nearly the same frequency of 0.30 MeV. Another explanation for the alignment gain observed in this band, based on the total Routhian (TRS) calculations with an approximate frequency dependence for the pairing gap Δ, was proposed recently by Wyss *et al.* [37]. In their interpretation, the g.s.b. (with $\gamma \approx -2°$) is crossed by the prolate $\nu(i_{13/2})^2$ configuration and, consecutively, by the triaxial $\nu(i_{13/2})^2$ configuration (the latter with $\gamma \approx -12°$ and ε_4 lower by ~ 0.02 than that in the g.s.b.). The crossing with two-quasiproton band is expected [27], instead, only at rotational frequencies higher than 0.34 MeV, or even higher than 0.64 MeV (Ref. [37]). The backbending observed in the g.s.b. in ^{180}Pt at a rotational frequency of $\hbar\omega \approx 0.32$ MeV, close to that of 0.30 MeV in the g.s.b. of ^{181}Ir, and with similar alignment gain, is also attributed to the alignment of a pair of $i_{13/2}$ neutrons [29], in agreement with the recent generator coordinator method (GCM) calculations [38] indicating that only $i_{13/2}$ neutrons are involved in the alignment process in the ^{180}Pt nucleus.

Therefore, it can be concluded, irrespective of the detailed mechanism involved, that the alignment of the $i_{13/2}$ neutron pair(s) is responsible for the backbending phenomena observed in this nuclear region at $\hbar\omega < 0.34$ MeV. The occupation of different proton configurations, on the other hand, results only in inducing considerable deformation changes causing, in turn, changes in the observed crossing frequencies, alignment gains, and interaction strength, as the crossing with two-quasiproton band is expected [36–38] only at much higher rotational frequencies. An especially important role is played by the occupation by an odd particle of the $h_{9/2}$, $\frac{1}{2}^-[541]$ proton configuration with a particularly strong driving force towards large ε_2 and slightly positive γ values (see discussion in the next section).

E. Systematics of band-crossing behavior in the Os-Pt region

The systematics of the experimental band-crossing frequencies in the ground-state bands of the even-even Os and Pt nuclei as well as in the one-quasiparticle bands in odd-A Ir and some bands in the odd-A Os nuclei, are shown in Fig. 5 as a function of the neutron number N. Similar systematics, as a function of the proton number Z, for $N = 104$ and 106 isotones, are shown in Fig. 6.

The critical frequency, $\hbar\omega_c$, of the neutron AB crossing, which is responsible for the backbending phenomena at rotational frequencies 0.25–0.35 MeV, is expected to rise with an increase in the quadrupole deformation and/or decrease in the hexadecapole deformation, as well as with the rise in the Fermi energy λ (see detailed discussion in Ref. [36]). Indeed, such a correlation can be noted in Fig. 5, where the calculated quadrupole and hexadecapole deformations [51] are shown in the lower part of the figure. Distinct changes in the band-crossing pattern observed for $N = 98$ and 108 and for $Z = 76$ (see Figs. 5 and 6) may be related to sudden changes of the Fermi energy due to pronounced gaps observed in single-particle level densities at these neutron and proton numbers, clearly indicating a connection between the observed backbending phenomena and the shell effects.

If γ deformations, or at least the γ stiffness, of the $\frac{1}{2}^-[541]$ orbital in the odd-A Ir isotopes and the Os cores are very close, as suggested by the EAR calculations (see Sec. IV C 2 and Table IV), only a difference in ε_2 and/or ε_4 may be responsible for the observed higher crossing frequencies in the $\pi h_{9/2}$ bands of Ir isotopes when compared to those in the respective Os cores, since a reduction in proton pairing in an odd-Z nucleus would not influence the neutron crossing frequencies. An equilibrium deformation calculation (with $\gamma = 0°$ assumed) for the $\frac{1}{2}^-[541]$ orbital and the even-even Os cores [52] gives $\Delta\varepsilon_2 \approx 0.011$, 0.020, and 0.026 for the $N = 104$, 106, and 108 pairs of isotones, respectively, with a nearly constant $\Delta\varepsilon_4 \approx -0.011$. It is not inconsistent with $\varepsilon_2(^{181}\text{Ir}) - \varepsilon_2(^{180}\text{Os}) \approx -0.01 \pm 0.02$, deduced from the measured [6] quadrupole moments Q_0, and with $\Delta\varepsilon_2 \approx 0.01$ and 0.02 for $N = 104$ and 108 pairs of isotones, respectively, as estimated from the $\mathcal{J}_0$ values of the ^{181}Ir and ^{185}Ir isotopes (which are higher by about $2\hbar^2$/MeV and $4\hbar^2$/MeV, respectively, than those of the corresponding Os cores). Consequently, one can expect shifts in the critical frequency of $\Delta\hbar\omega_c \approx 0.03$, 0.04, and 0.05 MeV for $N = 104$, 106, and 108 pairs of isotones, respectively, using the calculated $\Delta\varepsilon_2$ and $\Delta\varepsilon_4$ and an empirical relation

$$\Delta\hbar\omega_c \approx 1.32(\Delta\varepsilon_2) - 1.86(\Delta\varepsilon_4) \tag{11}$$

deduced from the experimental $\hbar\omega_c$ (AB) and calculated ε_2 and ε_4 (obtained from the recently calculated [53] β_2 and β_4 for $N = 94-106$, even-A Os isotopes). Therefore, a slightly higher quadrupole and, at the same time, a lower hexadecapole deformation of the $\frac{1}{2}^-[541]$ orbital may explain the observed shift in the crossing frequencies of the $\pi h_{9/2}$ bands in relation to the Os cores, $\Delta\hbar\omega_c$, of about 0.03 MeV for the $N = 104$ and 106 isotones, and account for about 60% of the shift (0.08 MeV) observed for the $N = 108$ isotones. The observed after-crossing alignment gains in relation to those observed in Os core isotopes are lower by about $\Delta i \approx 3\hbar$. It is not clear whether this decrease may also be explained by the aforementioned changes of quadrupole and hexadecapole deformation parameters. Recent TRS calculations for the even-even osmium isotopes with $N = 102-106$, also predict small negative γ values for low spin yrast states, decreasing to about $-12°$ after crossing with the S band, while the excited proton bands favor a minimum at $\gamma \geq 0°$. These differences in γ deformation may also contribute to the differences in crossing frequencies and after-crossing alignment observed in the pairs of Ir-Os isotones.

Careful reexamination of Routhians and the second moment of inertia, $\mathcal{J}^{(2)}$, plots for the g.s. bands reveals that, in addition to the distinct crossings at higher fre-

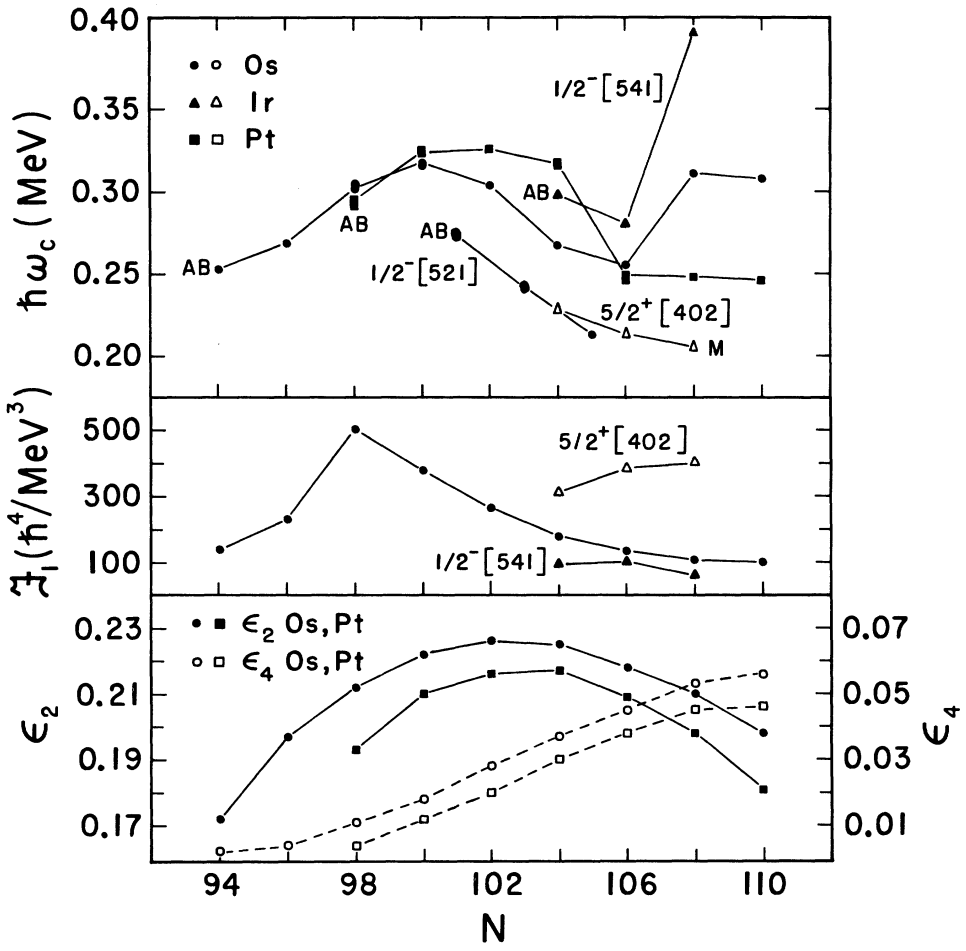

FIG. 5. (a) Systematics of the experimental band-crossing frequencies in the ground-state bands of the even Os and Pt nuclei and in the bands in odd-A Ir as well as in some bands in odd-A Os nuclei (the data are from Refs. [1, 2, 15, 16, 25–29, 35, 39–50]. The letters denote assumed character of the crossing. The vertical size of symbols represents roughly the strength of interaction: small backbending, medium upbending, and large-smooth upbending. (b) $\mathcal{J}_1$ parameter as deduced from the first three levels. (c) Calculated deformation parameters from Ref. [51].

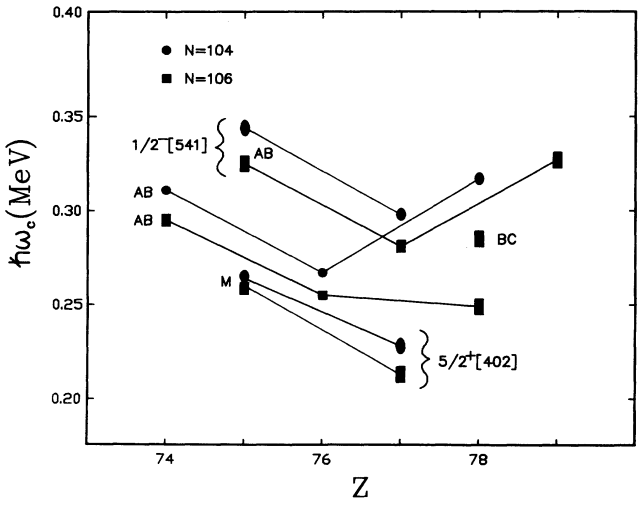

FIG. 6. Systematics of the experimental band-crossing frequencies in the $N=104$ and 106 isotones of the W, Re, Os, Ir, Pt, and Au nuclei. See Fig. 5 for explanations.

quencies, somewhat less obvious, smooth crossings (indicating a large interaction strength) also occur at $\hbar\omega < 0.25$ MeV in the $N=96-102$ Os isotopes [26,35,40]. Further, there is a substantial increase in the $\mathcal{J}_1$ values as deduced from the energies of the first two rotational states of the respective g.s. bands (middle part of Fig. 5). Two alternative explanations of this effect have been proposed: one involves a multistructure crossing, where several $\nu i_{13/2}$ quasiparticle alignments occur one after another in a narrow frequency range, accompanied by a rapid diminishing of the neutron pairing correlations over the frequency range 0.2–0.3 MeV (Ref. [35]); the second invokes an abrupt change of the γ deformation of the crossing $(\nu i_{13/2})^2$ aligned band, from an approximately prolate shape ($\gamma \approx 0°$) to a triaxial one with $\gamma \approx -12°$, whence the extra alignment gain gives rise to the observed irregularity in the alignment pattern (Ref. [37]). Since, in both interpretations, the low-frequency crossing discussed herein is a kind of "collective" phenomenon, the wave function of the crossing band is a nearly complete mixture of the wave functions of the $\nu i_{13/2}$

configurations with different K values (or, as in the hypothesis of the triaxial S band, K is no longer a good quantum number), we propose to call it the M (multistructure) crossing, in contradistinction from the "normal" crossing, where the mixed wave function of the crossing band is more clearly dominated by a single-K value. The experimental data (see Fig. 5) suggest that, with increasing $\hbar\omega_c$, such M crossings may smoothly change into "normal" crossings.

The low-frequency crossings observed in the $\frac{9}{2}^-[514]$ band in ^{181}Ir and the $\frac{5}{2}^+[402]$ bands in the odd-A $^{181-185}$Ir isotopes may also have a nature similar to the M crossings discussed above. In all these bands, smooth crossings (indicating large interactions with the crossing band) are evident in the 0.20–0.23 MeV frequency region; these are considerably lower than the observed crossing frequencies in the $\frac{1}{2}^-[541]$ bands of the neighboring even Ir isotopes as well as those in the ground-state bands of the neighboring even Os and Pt isotones (Fig. 5). The crossing frequencies in the $\frac{5}{2}^+[402]$ configuration decrease with N, in fair agreement with the Eq. (11) using the respective changes in the calculated [52] ε_2 and ε_4. However, the calculated deformation parameters for these bands are significantly larger than those for the $\frac{1}{2}^-[541]$ bands, in qualitative agreement with the observed differences of moments of inertia in the respective rotational bands, implying higher expected crossing frequencies, in contradiction with the experiment. Further, a reduction in proton pairing in an odd-Z nucleus should not affect the neutron crossing frequencies. Considerably larger hexadecapole deformation ε_4 (not predicted by the calculations), and/or significantly lower γ deformations of these orbitals ($\gamma < 0°$, as suggested in Ref. [46]) compared with the corresponding parameters for the $\pi h_{9/2}$ proton orbitals and the Os and Pt isotones, would be consistent with the observed low values of $\hbar\omega_c$. Therefore, the M crossing, analogous to that observed in the $N = 96-102$ even-A Os isotopes (note in Fig. 5 the especially close values of their $\hbar\omega_c$ and interaction strength, as estimated from $\mathcal{J}_1$, to those observed in the ^{176}Os and ^{178}Os), seems to be the only possible interpretation of these low-frequency crossings in odd-A Ir isotopes consistent with the available data.

If the above assumption is true, one would expect, taking $\Delta\hbar\omega$(AB-M) from Fig. 5 ($^{176-178}$Os region) at analogous M-crossing frequencies, that the next crossing would occur at frequencies of about 0.08, 0.10, and 0.11 MeV higher than the first crossing in these bands in ^{181}Ir, ^{183}Ir, and ^{185}Ir, respectively. Although the highest observed rotational frequencies, $\hbar\omega \approx 0.28$ MeV, in both bands in ^{181}Ir are too low to verify the predicted crossing at $\hbar\omega \approx 0.31$ MeV, the $\frac{5}{2}^+[402]$ band in ^{183}Ir indeed shows a hint of such a crossing at $\hbar\omega \approx 0.32$ MeV with $\Delta i \geq 9\hbar$, in excellent agreement with the predicted frequency of 0.314 MeV and alignment gain of $\approx 9\hbar$, strongly supporting the above assumption.

Values of $\hbar\omega_c$ for $\frac{1}{2}^-[521]$ rotational bands in the odd-N $^{177-181}$Os nuclei [44] are also lower than the corresponding values in neighboring even-N isotopes by about 0.05 MeV (see Fig. 5); this is very similar to the value of the aforementioned reduction in $\hbar\omega_c$ for the $\frac{9}{2}^-[514]$ and $\frac{5}{2}^+[402]$ bands in odd-Z Ir nuclei. However, these differences in $\hbar\omega_c$ have been interpreted as resulting from the reduction of the neutron pairing for odd-N nuclei relative to that in the even-N nuclei [54]. This interpretation is strongly supported by nearly the same reduction in the crossing frequencies in the ground-state band (with a $\pi\frac{1}{2}^-[541]$ configuration) in ^{182}Ir, as compared with the $\pi\frac{1}{2}^-[541]$ rotational band in ^{181}Ir (see discussion in Ref. [55]).

However, the low $\hbar\omega_c$ of M crossings observed in the $\frac{9}{2}^-[514]$ and $\frac{5}{2}^+[402]$ bands in the odd-A Ir nuclei cannot be explained by the same analogy since a reduction in proton pairing should not influence the neutron crossing frequencies. The difference in the backbending behavior between the $\frac{1}{2}^-[541]$ rotational band and both the $\frac{9}{2}^-[514]$ and $\frac{5}{2}^+[402]$ bands in the odd-A Ir isotopes may instead by attributed to differences in the deformations and a particle or hole character of the configurations involved. The low-frequency crossings, observed in the bands associated with the $\pi d_{5/2}$ $\frac{5}{2}^+[402]$ and $\pi h_{11/2}$ $\frac{9}{2}^-[514]$ configurations, have been interpreted as the $\nu i_{13/2}$ crossing shifted to a lower frequency as a result of negative-γ driving effects of these configurations [46,56]. This interpretation may be consistent with the proposed prolate triaxial ($\nu i_{13/2}$) S-band crossing [37] as well as with the multistructure crossing [35] because large negative-γ values (like large positive ε_4) bring the low-K, $i_{13/2}$ neutron configurations closer to each other, leading to a strong mixing of these configurations. Altogether, it would explain the observed low-frequency anomalies (the M crossings) in the $\frac{9}{2}^-[514]$ and $\frac{5}{2}^+[402]$ bands in odd-A Ir nuclei, as crossings with a multistructure (consisting of a strong mixture of the low-K, $\nu i_{13/2}$ configurations) neutron-aligned band with negative (and, possibly, decreasing with the rise in rotational frequency) γ deformation. Moreover, the wave functions of the crossing band may even be spread over different γ values with a concentration around $-15°$ to $4°$ at $\hbar\omega \approx 0.2$ MeV, as indicated by recent generator coordinator method calculations [38] for similar low-frequency crossings in ^{184}Pt. However, it is still an open question whether this interpretation can explain the considerably larger interaction strength of the proposed $\nu i_{13/2}$ crossing in the $\pi d_{5/2}$ and $\pi h_{11/2}$ bands compared to that in the $\pi h_{9/2}$ bands in Ir isotopes.

The occupation of the $h_{9/2}$ configuration with a particularly strong driving force by an odd proton (leading to a larger ε_2 and a slightly positive γ) has just the opposite effect, viz., shifting neutron crossing frequencies to much higher values and leading to the much simpler configuration structure for the S band ("normal" AB crossing). It is also consistent with vanishing of the M crossing when the $\frac{1}{2}^-[541]$ configuration is occupied by an odd proton, and with the conclusion (see Sec. IV C) that the alignment of the $i_{13/2}$ neutrons is small or negligible below the backbending region in the $h_{9/2}$ proton rotational bands in the odd-A Ir nuclei. Detailed TRS calculations in ε_2-, and ε_4-, and γ-parameter space, and an application of the generator coordinator method [38]

(which permits a description of the dynamics of the band crossings) to the rotational alignment process, are necessary to determine whether the explanation proposed above for the observed backbending behavior of the Ir isotopes is correct.

It is interesting to note that, in various rotational bands, the differences in the crossing frequencies and interaction strength between the $N=104$ and 106 isotones are lower than the corresponding differences between the neighboring isotopes (see Fig. 6). Therefore, it may be surmised that filling consecutive proton orbitals has a decisive influence on the backbending behavior of nuclei in the vicinity of $Z=77$ and $N=104$ due to the significant changes in the deformation parameters in the various quasiparticle configurations, as discussed above.

V. SUMMARY AND CONCLUSIONS

High spin states in the nucleus ^{181}Ir have been studied via ^{16}O-induced fusion-evaporation reaction. Four band structures have been identified. The mixed $h_{9/2}$ proton configurations form the yrast and yrare rotational bands. Model calculations as well as some experimental evidence indicate that the $\frac{1}{2}^-[541]$ and $\frac{3}{2}^-[532]$ Nilsson states, respectively, constitute the main components of the wave functions of these bands. Two other rotational bands, built on low-lying $\frac{5}{2}^+[402]$ and $\frac{9}{2}^-[514]$ isomeric states, have been observed. Analysis of the decay properties of the respective bandheads, as well as the gyromagnetic ratios, g_K, extracted from $M1/E2$ mixing ratios and the branching ratios in the associated rotational bands, support the proposed Nilsson quantum number assignments. In addition, two more band structures have been found. One of them deexcites to the yrast and yrare levels while the other is built on a short-lived, high spin isomer which decays through some intermediate levels to the $\frac{9}{2}^-[514]$ rotational band. The latter closely resembles the rotational bands built on the 7^- isomer in ^{180}Os and the 7^- state in ^{182}Pt, both in excitation energy and level spacing. Since the half-lives of the isomers in ^{181}Ir and ^{180}Os, as well as the deduced g_k factors, are also quite similar, it is suggested that the observed isomer has a $\{7^-\otimes\frac{9}{2}^-[514]\}_{23/2^+}$ configuration, decaying mainly through the 1882.1-keV state with a proposed $\{6^+\otimes\frac{9}{2}^-[514]\}_{21/2^-}$ configuration.

The axial (Nilsson model with pairing and Coriolis interaction included) and nonaxial (extended asymmetric rotor) model approaches have been applied to the $h_{9/2}$ proton level system. Both models give consistent results for the values of the moment of inertia, the Coriolis interaction attenuation, and the softness parameter. The experimental level energies are clearly better fitted by the EAR model, while the transition probabilities calculated in the framework of the $N+C$ model seem to be closer to the experimental values, although the differences lie within the experimental error bars in most cases. From the available experimental data, it has not been possible to reach a definite conclusion regarding the existence of a rigid nonaxial shape of the odd-A Ir nuclei in the ground state. Nonetheless, the EAR model may be an efficient way to take into account the dynamical γ deformation and/or softness, which are important for a clear understanding of the behavior of the rotational states in these nuclei.

The backbending pattern of the $\frac{1}{2}^-[541]$ rotational bands in odd-A Ir isotopes generally follows that of the respective even cores. Slightly higher crossing frequencies may be explained by somewhat different deformations of the $h_{9/2}$ configuration. These differences, however, cannot easily account for the observed differences in the after-crossing alignment gains which are considerably lower than in the g.s. rotational bands of the even-even cores. The nature of the low-frequency anomalies (the M crossings) observed in the g.s. bands of the $N=96-102$ Os isotopes, and in the $\frac{5}{2}^+[402]$ and $\frac{9}{2}^-[514]$ rotational bands in odd-A Ir isotopes has been extensively discussed. A crossing with a multistructure, neutron-aligned band, with sizable negative γ and positive ε_4 mean deformations, is proposed in order to explain this phenomenon.

The important role played by the occupation of strongly deformation driving $\frac{1}{2}^-[541]$ configuration by one or two protons in inducing deformation changes that lead, in turn, to different backbending behavior in this nuclear region has been explored. Even small deformation changes may lead to changes, relative to Fermi energy, in the position of high-j, low-K orbitals which play a decisive role in the backbending phenomena. Not only can the ε_2, ε_4, and γ deformation parameters be configuration dependent, but also the softness of nucleus toward changes in these parameters may depend on configuration, leading to different behavior of the rotational bands built on various configurations. Detailed TRS calculations in the ε_2-, ε_4-, and γ-parameter space and GCM calculations (for a description of the dynamics of the band crossings) are vital for a more complete understanding of the observed backbending behavior of the Os-Pt isotopes.

ACKNOWLEDGMENTS

One of the authors (R.K.) would like to express his gratitude to the staff of the Physics Department of the University of Notre Dame for their warm hospitality during his stays at Notre Dame. This work has been supported in part by the National Science Foundation (Grant Nos. PHY82-00426 and PHY88-03035) and the Polish Central Project for Fundamental Research CPBP 01.09.

[1] S. André, J. Genevey-Rivier, J. Treherne, J. Jastrzebski, R. Kaczarowski, and J. Lukasiak, Phys. Rev. Lett. **38**, 327 (1977).

[2] S. André, J. Genevey-Revier, J. Treherne, R. Kaczarowski, J. Lukasiak, and J. Jastrzebski, Nucl. Phys. **A325**, 445 (1979).

[3] S. André, J. Boutet, J. Rivier, J. Treherne, J. Jastrzebski, J. Lukasiak, and Z. Suijkowski, Nucl. Phys. **A243**, 229 (1975).

[4] J. Lukasiak, R. Kaczarowski, J. Jastrzebski, S. André, and

J. Treherne, Nucl. Phys. **A313**, 191 (1979).
[5] U. Garg, E. R. Marshalek, A. Chaudhury, E. G. Funk, R. Kaczarowski, J. W. Mihelich, D. Frekers, R.V.F. Janssens, D. Radford, and A. M. van den Berg, Phys. Lett. **151B**, 335 (1985).
[6] R. Kaczarowski, U. Garg, A. Chaudhury, E. G. Funk, J. W. Mihelich, D. Frekers, R.V.F. Janssens, and T. L. Khoo, Phys. Rev. C **41**, 2069 (1990).
[7] C. Schück, A. Knipper, C. Richard-Serre, V. Berg, A. Zerrouki, J. Genevey-Rivier, and the ISOLDE Collaboration, in *Future Directions in Studies of Nuclei Far from Stability,* edited by J. H. Hamilton *et al.* (North-Holland, Amsterdam, 1980), p. 127.
[8] A. J. Kreiner, J. Davidson, M. Davidson, P. Thieberger, and E. K. Warburton, Phys. Rev. C **42**, 878 (1990).
[9] E. der Mateosian and A. W. Sunyar, At. Data Nucl. Data Tables **13**, 391 (1974); **13**, 407 (1974).
[10] A. Bohr and B. Mottelson, Nuclear Structure, Vol. 2 (Benjamin, Reading, Mass. 1975).
[11] H. Rubinsztein and M. Gustafsson, Phys. Lett. **58B**, 283 (1975).
[12] C. Ekström, H. Rubinsztein, and P. Möller, Phys. Scr. **14**, 189 (1976).
[13] A. Visvanathan, E. F. Zganjar, J. L. Wood, R. W. Fink, L. L. Riedinger, and F. E. Turner, Phys. Rev. C **19**, 282 (1979).
[14] F. Rösel, H. M. Fries, K. Alder, and H. C. Pauli, At. Data Nucl. Data Tables **21**, 291 (1978).
[15] Ts. Venkova, T. Morek, R. M. Lieder, W. Gast, G. Hebbinghaus, A. Krämer-Flecken, W. Urban, G. Sletten, and K. H. Maier, Z. Phys. A **334**, 385 (1989).
[16] A. Neskakis, R. M. Lieder, M. Möller-Vegian, H. Beuscher, W. F. Davidson, and C. Mayer-Böricke, Nucl. Phys. **A261**, 189 (1976).
[17] C. Schück, J. Genevey-Rivier, V. Berg, A. Knipper, G. Walter, C. Richard-Serre, and A. Höglund, Nucl. Phys. **A325**, 421 (1979).
[18] E. Browne, Nucl. Data Sheets **55**, 483 (1988).
[19] *Table of Isotopes,* edited by C. M. Lederer, J. M. Hollander, and I. Perlman (Wiley, New York, 1978).
[20] V. P. Janzen, M. P. Carpenter, L. L. Riedinger, W. Schmitz, S. Pilotte, S. Monaro, D. D. Rajnauth, J. K. Johansson, D. G. Popescu, J. C. Waddington, Y. S. Chen, F. Dönau, and P. B. Semmes, Phys. Rev. Lett. **61**, 2073 (1988).
[21] A. Bohr and B. Mottelson, *Nuclear Structure* (Benjamin, New York, 1969), Vol. 1.
[22] A. S. Goldhaber and G. Scharff-Goldhaber, Phys. Rev. C **17**, 1171 (1978).
[23] O. Prior, F. Boehm, and S. G. Nilsson, Nucl. Phys. **A110**, 257 (1968).
[24] W. Nazarewicz, private communication.
[25] C. L. Dors, F. M. Bernthal, T. L. Khoo, C. H. King, J. Borggreen, and G. Sletten, Nucl. Phys. **A314**, 61 (1979).
[26] G. D. Dracoulis, C. Fahlander, and M. P. Fewell, Nucl. Phys. **A383**, 119 (1982).
[27] R. M. Lieder, A. Neskakis, J. Skalski, G. Sletten, J. D. Garrett, and J. Dudek, Nucl. Phys. **A476**, 545 (1988).
[28] W. Schmitz, M. P. Carpenter, L. H. Courtney, V. P. Janzen, L. L. Riedinger, K. Johannsson, G. Kajrys, D. Popescu, J. C. Waddington, J. DeBuc, S. Monaro, and S. Pilotte. ISKP, University of Bonn Annual Report, 1987.
[29] M. J. A. de Voigt, R. Kaczarowski, H. J. Riezebos, R. F. Noorman, J. C. Bacelar, M. A. Delaplanque, R. M. Diamond, F. S. Stephens, J. Sauvage, and B. Boussière, Nucl. Phys. **A507**, 472 (1990).
[30] M. J. A. de Voigt, R. Kaczarowski, H. J. Riezbos, R. F. Noorman, J. C. Bacelar, M. A. Delaplanque, R. M. Diamond, and F. S. Stephens, Nucl. Phys. **A507**, 447 (1990).
[31] S. G. Nilsson, Chin Fu Tsang, A. Sobiczewski, Z. Szymanski, S. Wycech, C. Gustafson, I.-L. Lamm, P. Möller, and B. Nilsson, Nucl. Phys. **A131**, 1 (1969).
[32] R. Kaczarowski, Comput. Phys. Commun. **13**, 63 (1977).
[33] J. Meyer ter Vehn, Nucl. Phys. **A249**, 111 (1975); **A249**, 141 (1975).
[34] R. Kaczarowski and J. Lukasiak (unpublished).
[35] J. C. Wells, N. R. Johnson, C. Baktash, I. Y. Lee, F. K. McGowan, M. A. Riley, A. Virtanen, and J. Dudek, Phys. Rev. C **40**, 725 (1989).
[36] R. Bengtsson, S. Frauendorf, and F. R. May, At. Data Nucl. Data Tables **35**, 15 (1986).
[37] R. Wyss, W. Satuła, W. Nazarewicz, and A. Johnson, Nucl. Phys. **A511**, 324 (1990).
[38] J.-Y. Zhang, F. Dönau, and L. L. Riedinger, Phys. Rev. C **42**, 1436 (1990).
[39] G. D. Dracoulis, R. A. Bark, A. E. Stuchbery, A. P. Byrne, A. M. Baxter, and F. Riess, Nucl. Phys. **A486**, 414 (1988).
[40] B. Fabricius, G. D. Dracoulis, R. A. Bark, A. E. Stuchbery, T. Kib, and A. M. Baxter, Nucl. Phys. **A511**, 345 (1990).
[41] G. D. Dracoulis, T. Kibdi, A. P. Byrne, B. Fabricius, and A. E. Stuchbery, Nucl. Phys. **A509**, 605 (1990).
[42] R. M. Lieder, G. Sletten, J. Borggreen, and J. Pedersen, Nucl. Phys. **A375**, 291 (1982).
[43] R. Spanhoff, H. Postma, and M. J. Canty, Phys. Rev. C **18**, 111 (1978).
[44] G. D. Dracoulis, C. Fahlander, and A. P. Byrne, Nucl. Phys. **A401**, 490 (1983).
[45] G. D. Dracoulis, A. E. Stuchbery, A. P. Byrne, A. R. Poletti, S. J. Poletti, J. Gerl, and R. A. Bark, J. Phys. G **12**, L97 (1986).
[46] M. P. Carpenter *et al.*, Nucl. Phys. **A513**, 125 (1990).
[47] G. Hebbinghuas, W. Gast, A. Krämer-Flecken, R. M. Lieder, J. Skalski, and W. Urban, Z. Phys. A **328**, 387 (1987).
[48] M. Piiparinen, J. C. Cunnane, P. J. Daly, C. L. Dors, F. M. Bernthal, and T. L. Khoo, Phys. Rev. Lett. **34**, 1110 (1975).
[49] A. J. Larabee, M. P. Carpenter, L. L. Riedinger, L. H. Courtney, J. C. Waddington, V. P. Janzen, W. Nazarewicz, J.-Y. Zhang, R. Bengtsson, and G. A. Leander, Phys. Lett. **169B**, 21 (1986).
[50] D. L. Balabanski, W. Gast, G. Hebbinghaus, A. Krämer-Flecken, R. M. Lieder, T. Morek, T. Rzaca-Urban, H. Schnare, and W. Urban, Z. Phys. A **332**, 111 (1989).
[51] I. Ragnarsson, A. Sobiczewski, R. K. Sheline, S. E. Larsson, and B. Nerlo-Pomorska, Nucl. Phys. **A233**, 329 (1974).
[52] R. Kaczarowski and W. Nazarewicz, INR Progress report, 1982.
[53] W. Nazarewicz, M. A. Riley, and J. D. Garrett, Nucl. Phys. **A512**, 61 (1990).
[54] J. D. Garrett and S. Frauendorf, Phys. Lett. **108B**, 77 (1982).
[55] A. J. Kreiner, Nucl. Phys. **A520**, 225c (1990).
[56] L. L. Riedinger, Nucl. Phys. **A520**, 287c (1990).